HHS Public Access

Author manuscript

*Cell Stem Cell*. Author manuscript; available in PMC 2024 March 05.

Published in final edited form as:

*Cell Stem Cell*. 2023 November 02; 30(11): 1434–1451.e9. doi:10.1016/j.stem.2023.10.002.

# Development of functional resident macrophages in human pluripotent stem cell-derived colonic organoids and human fetal colon

**Jorge O. Múnera**[1,2,12,13,*], **Daniel O. Kechele**[1,12], **Carine Bouffi**[3], **Na Qu**[2], **Ran Jing**[4,5], **Pritiprasanna Maity**[2], **Jacob R. Enriquez**[1], **Lu Han**[6], **Ian Campbell**[1], **Maxime M. Mahe**[3], **Heather A. McCauley**[1], **Xinghao Zhang**[1], **Nambirajan Sundaram**[3], **Jonathan R. Hudson**[1], **Adrian Zarsozo-Lacoste**[1], **Suman Pradhan**[7], **Kentaro Tominaga**[1], **J. Guillermo Sanchez**[1], **Alison A. Weiss**[7], **Praneet Chatuvedi**[1], **Jason R. Spence**[8], **Mariam Hachimi**[4], **Trista North**[4], **George Q. Daley**[4,5], **Christopher N. Mayhew**[1,9], **Yueh-Chiang Hu**[1,9], **Takanori Takebe**[1,10], **Michael A. Helmrath**[3,10], **James M. Wells**[1,10,11,*]

[1]Division of Developmental Biology, Cincinnati Children's Hospital Medical Center, Cincinnati, OH 45229-3039, USA

[2]Department of Regenerative Medicine and Cell Biology, Medical University of South Carolina, Charleston, SC 29425, USA

[3]Division of Pediatric General and Thoracic Surgery, Cincinnati Children's Hospital Medical Center, Cincinnati, OH, USA

[4]Stem Cell Program, Boston Children's Hospital, Boston, MA, USA

[5]Department of Biological Chemistry and Molecular Pharmacology, Harvard Medical School, Boston, MA, USA

[6]Department of Biochemistry and Molecular Biology, Hollings Cancer Center, Medical University of South Carolina, Charleston, SC, USA

[7]Department of Molecular and Cellular Physiology, University of Cincinnati, Cincinnati, OH 45267, USA

[*]Correspondence: munera@musc.edu (J.O.M.), james.wells@cchmc.org (J.M.W.).

AUTHOR CONTRIBUTIONS

J.O.M., D.O.K., and J.M.W. conceived the study and experimental design, performed and analyzed the experiments, and co-wrote the manuscript. C.B., N.Q., P.M., L.H., A.Z.-L., I.C., M.M.M., H.A.M., N.S., J.R.H., K.T., T.T., and M.A.H. aided in or performed experiments. R.J., M.H., T.N., and G.Q.D. performed validation experiments. D.O.K., J.R.E., P.C., X.Z., and J.G.S. performed bioinformatic analysis of bulk RNA-seq or scRNA-seq data. S.P. and A.A.W. performed bacterial microinjections into HCOs. C.N.M. and Y.-C.H. designed and generated the CDX2 CRISPR iPSC line. J.R.S. provided human fetal colon scRNA-seq datasets and technical support. All authors contributed to the editing of the manuscript.

SUPPLEMENTAL INFORMATION

Supplemental information can be found online at https://doi.org/10.1016/j.stem.2023.10.002.

DECLARATION OF INTERESTS

The authors declare no competing interests.

INCLUSION AND DIVERSITY

We support inclusive, diverse, and equitable conduct of research. One or more of the authors of this paper self-identifies as an underrepresented ethnic minority in their field of research or within their geographical location. One or more of the authors of this paper received support from a program designed to increase minority representation in their field of research.

[8]Division of Gastroenterology and Hepatology, Department of Internal Medicine, University of Michigan Medical School, Ann Arbor, MI 48109, USA

[9]Pluripotent Stem Cell Facility, Cincinnati Children's Hospital Medical Center, Cincinnati, OH, USA

[10]Center for Stem Cell and Organoid Medicine (CuSTOM), Cincinnati Children's Hospital Medical Center, Cincinnati, OH, USA

[11]Division of Endocrinology, Cincinnati Children's Hospital Medical Center, Cincinnati, OH, USA

[12]These authors contributed equally

[13]Lead contact

## SUMMARY

Most organs have tissue-resident immune cells. Human organoids lack these immune cells, which limits their utility in modeling many normal and disease processes. Here, we describe that pluripotent stem cell-derived human colonic organoids (HCOs) co-develop a diverse population of immune cells, including hemogenic endothelium (HE)-like cells and erythromyeloid progenitors that undergo stereotypical steps in differentiation, resulting in the generation of functional macrophages. HCO macrophages acquired a transcriptional signature resembling human fetal small and large intestine tissue-resident macrophages. HCO macrophages modulate cytokine secretion in response to pro- and anti-inflammatory signals and were able to phagocytose and mount a robust response to pathogenic bacteria. When transplanted into mice, HCO macrophages were maintained within the colonic organoid tissue, established a close association with the colonic epithelium, and were not displaced by the host bone-marrow-derived macrophages. These studies suggest that HE in HCOs gives rise to multipotent hematopoietic progenitors and functional tissue-resident macrophages.

## Graphical abstract

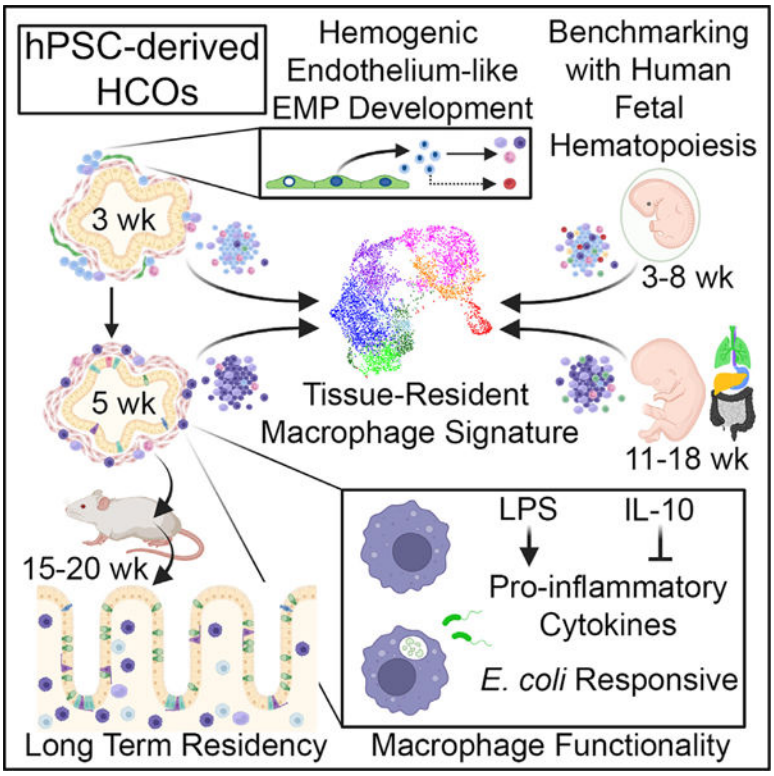



## In brief

Múnera, Kechele, and colleagues report the generation of pluripotent stem cell (PSC)-derived human colonic organoids (HCOs) with co-developing macrophages resembling resident macrophages in the human fetal colon. BMP signaling induces hemogenic-endothelium-like cells that give rise to erythromyeloid progenitors that differentiate into functional macrophages that persist after the transplantation of HCOs.


## INTRODUCTION

Diverse populations of immune cells, both myeloid and lymphoid, populate the adult gastrointestinal (GI) tract. Most intestinal diseases, particularly inflammatory bowel diseases (IBDs), involve the immune system. Historically, it was thought that most immune cells of the gut, including resident macrophages, arise from bone-marrow-derived hematopoietic stem cells (HSCs).[1] However, animal studies support the conclusion that many organs contain a population of tissue-resident macrophages that arise independently of HSCs during embryonic development.[2–5] Seminal work using lineage tracing in mice demonstrated that tissue-resident macrophages of many organs are derived from fetal pre-macrophages.[6] The murine small intestine and colon contain stable, self-maintaining populations of macrophages derived from both embryonic progenitors and adult HSCs.[7–10] The embryonic development of tissue-resident macrophages within the human fetal colon has not been described.

During murine embryonic development, hematopoietic cells are generated in three waves.[11,12] In the first wave, primitive hematopoietic cells arise during gastrulation within the yolk sac; co-express endothelial, erythroid (ErP), and macrophage markers; and are short lived, except for microgia.[13] The second, pro-definitive wave gives rise to hematopoietic progenitor cells (HPCs) originating from hemogenic endothelium (HE) in several extraembryonic and intraembryonic sites, including the yolk sac, placenta, umbilical cord, and para-aortic splanchnopleure.[14–17] Adjacent to the developing colon, the aorta-gonad-mesonephros (AGM) region of the embryo proper is one of the predominant sites for the formation of HPCs, which arise from the endothelial-to-hematopoietic transition (EHT) of RUNX1+ ventral HE cells.[18] Although initially these HPCs were thought to have only erythromyeloid differentiation potential, studies have now suggested that they are capable of lymphoid differentiation.[16,19,20] It is thought that HPCs from the yolk sac and possibly the AGM can beget self-renewing resident macrophages in tissues such as those in the lungs and liver.[2] Through human fetal single-cell RNA sequencing (scRNA-seq) analysis, it is now hypothesized that a subset of HPCs acts as nascent or pre-HSCs, which can migrate into the fetal liver and mature into HSCs prior to populating the bone marrow.[16,17] These third, definitive wave HSCs populate the bone marrow and become long-lived HSCs.[21–24]

Despite separate progress in the derivation of immune cell types[25–32] and organoids[33–41] from human pluripotent stem cells (hPSCs), the development of human GI organoids containing co-developing tissue-resident immune cells has remained elusive. Here, we report the differentiation of hPSCs into human colonic organoids (HCOs) containing HE-like cells and an array of hematopoietic cell types. Transcriptional comparison with developing hematopoietic cells from human embryos suggests that HCOs contain an HPC-like population giving rise to a robust population of myeloid cell types that primarily differentiate through granulocyte-monocyte progenitors (GMPs) and myeloblast and monocyte intermediates toward the macrophage lineage. These HCO-derived macrophages acquire a fetal, posterior-GI-enriched transcriptional signature comparable to human fetal colon tissue-resident macrophages. HCO macrophages are functional and can mount a robust response to inflammatory cues such as pathogenic *E. coli*. Finally, these hPSC-derived macrophages co-develop with HCOs over several months *in vivo* and are not displaced by bone-marrow-derived macrophages from the host; rather, both sources contribute to the colonic organoid. These data describe an approach to generate human organoid tissues with co-developing resident immune cells that could be used to model inflammatory diseases and the developmental roles of tissue-resident immune populations.

## RESULTS

### HCO mesenchyme contains HE-like cells

We previously developed methods to generate human intestinal organoids[37] (HIOs) and HCOs[36] through the directed differentiation of hPSCs. The transient activation (HCO) or inhibition (HIO) of BMP signaling was sufficient to stably pattern mid/hindgut (HG) cultures into the resulting organoids[36] (Figure S1A). HCOs contained colonic epithelium and surrounding mesenchymal derivatives, including fibroblasts, myofibroblasts, and smooth muscle cells. However, we found that combining BMP activation with the subsequent

growth of nascent HCO spheroids at high density resulted in the emergence of an immune-related transcriptional signature by day 21 (Figures S1B and S1C). Since the main source of hematopoietic cells during development is HE, we investigated whether HCOs contained HE-like cells. Given that BMP signaling is required for the development of this posterior and ventral region of the embryo,[36,42–44] we postulated that BMP manipulation generated a ventral caudal, AGM-like mesoderm. In fact, BMP-treated spheroids expressed a posterior HOX code (Figure S1D). Similar to what has been described in HIOs,[45] HCOs had co-developing cells that expressed endothelial markers as early as day 10 (Figures S1E and S1G). Importantly, HCOs had a reduced expression of venous markers and were enriched for arterial markers, compared with HIOs. Additionally, HCOs had an increased expression of GATA2, which is normally observed in the AGM[46] (Figures S1E–S1H). This expression pattern in HCOs is consistent with ventral arterial endothelium, supporting enhanced HE-like potential.

RUNX1 marks HPCs emerging from HE.[27,47–49] In E10.5 mouse embryos, endothelial cells in the AGM region contained clusters of emerging RUNX1+ HPCs (Figure 1A). Both day 21 HIO and HCO cultures contained CD34+ endothelial tubes, but only HCOs co-expressed RUNX1 (Figures 1B and 1C). Shortly after the emergence of RUNX1+ HPCs, hematopoietic lineages differentiate and circulate throughout the embryo. Similarly, in HCO cultures, light microscopy revealed highly refractory cells that push through endothelial-like tubes and emerge to accumulate in the cell culture medium (Figure 1D; Video S1). These refractory cells were observed in 94.7% ± 4.6% of wells containing HCOs and none of the HIO wells (Figure 1E). Consistent with the presence of RUNX1+ cells, SPI1/PU.1+ hematopoietic cells were prevalent in HCO cultures and absent in HIOs (Figures 1F and 1G). Bulk RNA-seq further supported the enhanced expression of hematopoietic markers, including *RUNX1*, *PTPRC/CD45*, *SPI1*, *SPN/CD43*, *MYB*, and *GFI1*, in day 21 HCO cultures, but not in HIO cultures (Figures 1H and S1B). Finally, CD34+ cells were isolated from day 21 HCOs and shown to undergo an EHT-like process (Figures 1I and 1J). Collectively, these data indicate that HCO cultures contain HE-like and associated RUNX1+ cells (Figure 1K).

## HE-like and hematopoietic progenitors in HCO cultures resembled first trimester human fetal hematopoiesis

To characterize the hematopoietic potential in HCO cultures, we performed transcriptional, morphological, and functional analyses (Figures 2A and S1A). Giemsa staining of cytospun cells harvested from the media of day 21–28 HCOs identified predominately immune progenitors and monocyte- and macrophage-like cells, with rare neutrophil-, eosinophil-, and basophil-like cells (Figures 2B and 2C). This along with bulk RNA-seq (Figure 1H) suggests that HCO cultures could support myeloid differentiation. Erythrocytes and lymphocytes were not detected in cytospins. To check for erythromyeloid progenitors (EMPs) in HCOs, we performed Methocult assays and found that HCO cultures, but not HIO cultures, contained progenitors that formed ErP, myeloid, and mixed myeloid (MM) colonies (Figures 2D and 2E). HCOs generated from human embryonic stem cells and multiple induced pluripotent stem cell (iPSC) lines gave rise to erythromyeloid derivatives, demonstrating the method's robustness (Figure 2E). Erythrocytes from Methocult expressed

hemoglobin genes, including pan (*HBA1*), embryonic (*HBE1*), fetal (*HBG1* and *HBG2*), and adult (*HBB*) genes, but the transcripts were predominantly *HBG1/2* and not *HBE1* or *HBB* subunits (Figure 2F). This hemoglobin distribution is consistent with 2nd wave definitive EMP but not with primitive or 3rd wave HSC hematopoiesis (Figure 2G).

Recent publications have mapped hematopoiesis during human fetal development. To identify the ontogeny of hematopoietic cells in HCOs, we performed scRNA-seq on HCO cultures from day 22, when these cells are abundantly detected (Figure S2A), and compared them with these human fetal atlases. We identified *PDGFRA* myofibroblasts, rare *CDH5*-expressing endothelial cells, and abundant hematopoietic cells in these cultures (Figures S2B and S2C). Mesenchyme and hematopoietic populations expressed a medial and posterior HOX code. Endothelial cells expressed markers consistent with mixed arterial/venous identity, Notch responsiveness, and were negative for *NT5E/CD73*, a signature that is consistent with HE (Figures S2G and S2H).[50] *CD34+RUNX1+* hematopoietic progenitors received signals that promote EHT, including NOTCH, WNT, KIT, transforming growth factor b (TGF-b), and hedgehog ligands (Figures S2D–S2F). *CD34+RUNX1+*-expressing cells downregulated endothelial genes and upregulated hematopoietic genes (Figures S2H and S2I). HCO immune cells did not appear to originate from primitive hematopoiesis, since primitive immune cells express *KDR+ GYPA/CD235a* mesoderm and bypass *MYB+* myeloid intermediates.[3,15,19] Moreover, primitive hematopoietic cells co-express fetal hemoglobin *HBE1* and *HBA1*, endothelial *CDH5*, and macrophage markers *CSF1R* and *CD163* (Figure 2G).[15,17,19,26] HCO immune cells did not display any of these features, and most hematopoietic cells at day 22 did not yet express macrophage markers (Figures S2H and S2I). These data indicate that immune cells in HCO cultures do not resemble those arising from primitive hematopoiesis.

To closely examine hematopoietic populations, we re-clustered *PTPRC/CD45*-expressing cells and identified 5 clusters (Figure 2H). These immune cells seemingly differentiate from *CD34+*-expressing progenitors to *MYB+ MPO+*-expressing GMPs to *LYZ+ S100A9+*-expressing myeloblast-like cells to *ITGAM/CD11b+ FCGR3A/CD16+ FCGR2A/CD32+ CSF1R+* monocyte-like cells (Figure 2I). The CD34+-expressing progenitor cluster also expressed *SPINK2*, *MLLT3*, *MECOM*, and *ANGPT1*, and rare cells also expressed *HOXA9* and *HLF* (Figure 2I), which is reminiscent of a human fetal nascent HSC signature.[16,17] Furthermore, *CD34+RUNX1+SPINK2+* progenitors from numerous extraembryonic and intraembryonic hemogenic sources have now been shown to have lympho-myeloid differentiation potential prior to the emergence of HSCs.[15,16,19] HCO cultures contained a similar population of cells that express markers of lymphocyte precursors and lack the expression of *SPN/CD43* (Figure 2K). Together, the early hematopoietic progenitors and lineages observed in HCOs faithfully resembled those observed during early hematopoiesis in human embryos.

## HCO hematopoietic progenitors reflected those found in human yolk sac and AGM

The human fetal scRNA-seq atlases compared hematopoiesis in different sites and Carnegie stages (CSs). We found that the hematopoietic progenitors in day 22 HCO cultures transcriptionally resembled the yolk sac multipotent progenitors (YSMPs), the nascent

pre-HSC HPC, or the multipotent progenitors (MPPs) from those atlases.[15,16,51] Using the Calvanese et al. CS14 tissues as a training dataset,[16] we utilized random forest (RF) and support vector machine (SVM) learning algorithms and ensemble to deduce the relationship between hemogenic sites and all the day 22 HCO immune cells. Although there was no clear consensus between the algorithms, together they indicated that day 22 HCO immune cells most closely approximated CS14 AGM, vitelline vessels, and liver (Figure 2L). We also integrated these datasets together to examine the ontogeny of the *CD34+RUNX1+SPINK2+* progenitor population (Figures S3A–S3D). The progenitors and cell proportions per cluster in day 22 HCOs were the most similar to the AGM and were distinct from liver and head progenitors (Figures S3D and S3E). Markers further support similarity to the reported nascent HSC *SPINK2* signature rather than the liver/head *SPINK2* signature, which represents lympho-myeloid progenitors (Figures S3G–S3I). Based on this more limited progenitor training dataset and Pearson correlations, the day 22 progenitors were the most similar to yolk sac and AGM progenitors (Figures S3J and S3K). Together, the transcriptional identity of the day 22 HCO immune progenitors and populations appears to accurately reflect a 1$^{st}$ trimester fetal developmental state and an ontogeny-like AGM and yolk sac.

## CDX2 is required for the generation of hematopoietic cells in HCOs

*Ex vivo* cultures of mouse AGM and HG revealed that signals from the HG/embryonic colon promote the development of HPCs from HE.[52] To determine whether HG patterning is necessary for the development of HE-like cells within HCO cultures, we generated organoids from control and caudal-type homeobox protein 2 (CDX2)-deficient iPSCs (CDX2 knockout [KO]), since endodermal *Cdx2* is required for development of the mouse HG.[53] No hematopoietic cells were observed in CDX2-KO-derived HCOs compared with wild-type (WT) control (Figures S4A and S4B). Consistent with previous reports, CDX2-KO-derived HCOs lost the expression of intestinal markers and ectopically expressed gastric markers (Figures S4C–S4F).[53–55] CDX2 also patterns mesenchyme and activates the medial/posterior HOX code, including in the HE.[56,57] CDX2-KO-derived HCOs had significantly reduced levels of the posterior HOX factors and lacked the expression of hematopoietic markers compared with control HCOs (Figure S4F). No endothelial-like tubes or hematopoietic cells were observed in day 22 CDX2-KO-derived HCOs (Figure S4G). Furthermore, Methocult assays of floating mesenchymal cells from control and CDX2-KO-derived HCOs revealed a loss of erythromyeloid potential in the latter (Figure S4H). Collectively, these data indicate that CDX2 is required for the generation of endothelium and EMPs in HCO cultures, consistent with a previous murine study.[58]

## The differentiation trajectory of macrophages in HCOs mirrored the trajectory of macrophages in human embryos

Lineage-tracing studies in mice demonstrate that pre-macrophages and fetal monocytes can colonize organs early in development and give rise to tissue-resident macrophages that persist until birth[59] and throughout life.[5,13] Although it is not possible to perform lineage-tracing experiments in humans, single-cell analysis of developing myeloid cells during human embryogenesis have mapped out the developmental trajectory of the myeloid lineages. To determine whether HCO-associated hematopoietic cells differentiate into

macrophages resembling their counterparts in human embryos, we performed scRNA-seq analysis of three different time points of HCO-macrophage development, namely day 22, day 28, and day 37 (Figure S1A). The three time points clustered in a continuum, with a clear progression from progenitor to macrophage (Figures 3A–3F). This progression was evident in automated cluster annotation based on a published fetal macrophage atlas[15] where the day 22 time point contained primarily YSMPs, GMPs, and myeloblasts, whereas monocyte and macrophage populations were largely present at day 28 and day 37, respectively (Figures 2H, 2I, 3B, 3C, and 3E). The progression was also supported by pseudotime analysis, which revealed a relatively linear differentiation trajectory (Figure 3D). The multipotent YSMP population was lost from day 22 to day 28 as cells committed to myeloid lineage, but some *CD163*+ cells at day 37 were cycling and clustered with myeloblasts/GMPs, suggesting potential for self-renewal (Figures 3C, 3E, and 3F). Consistent with a predominately myeloid and macrophage differentiation bias, CellChat cell-cell communication inference supported the notion that CSF1 was endogenously expressed by mesenchymal cells and acted on early hematopoietic cells (Figure S2D). The day 37 HCO-derived macrophages expressed a similar set of markers to those expressed by hPSC-derived monocytes/macrophages generated using the STEMdiff Hematopoietic Kit with subsequent macrophage colony stimulating factor (M-CSF) and GM-CSF treatment (Figure 3E).

Recent scRNA-seq analysis of 1$^{st}$ trimester human fetal hematopoiesis revealed that most cells were macrophages and their precursors (Figures 3G–3J).[10–12] No distinct lymphocyte populations were represented at these fetal stages, except for *CD7*-high lymphoid-myeloid progenitors. Comparing HCO cells with this atlas and two additional fetal hematopoietic atlases,[51,57] we found that the HCO hematopoietic cells differentiated predominately to the monocyte/macrophage lineage (Figures 3K and 3L). Fetal macrophages clustered differently based on mitotic status and enriched markers, with mitotic macrophages more prevalent in the yolk sac and expressing higher levels of *CX3CR1*, *CCR2*, *MRC1*, and *LYVE1* (Figures 3H–3J). By contrast, the G1/G0 macrophages were more prevalent in all fetal tissues and the day 28 and day 37 HCO cultures, and they expressed higher levels of *CD163*, *FOLR2*, and *ADAMDEC1*. In addition, the mitotic macrophages clustered closer to the *CD7*-low population and further from the GMP/myeloblast/monocyte intermediates, indicating that they could have a distinct differentiation trajectory. Consistent with this, relatively few cells from the CS14 fetal yolk sac and vitelline vessels clustered with GMP and myeloblast intermediates in this integrated analysis (Figures 3G–3I). By contrast, a larger proportion of cells from the CS14 AGM, umbilical cord, and liver clustered with GMP and myeloblast intermediates, which are predominately composed of cells from day 22 HCOs. Collectively, the differentiation of hematopoietic progenitors into macrophages in HCOs transcriptionally resembles human fetal hematopoiesis and similarly displays a myeloid differentiation bias.

## HCO macrophages adopted an expression signature resembling that of human fetal intestinal and colonic tissue-resident macrophages

Tissue-resident macrophages have molecular and functional features that distinguish them from bone marrow-derived macrophages. For example, CD163 is expressed in tissue-resident macrophage populations, including Hofbauer cells in the placenta, Kupffer cells

in the liver, and alveolar and colonic macrophages.[60–62] We identified that HCOs contained CD163+ macrophages, using human colon biopsies as a positive control (Figure 4A). By contrast, HIOs did not have CD163+ cells, consistent with the absence of HE (Figures 4A and 4B). Macrophages were observed in HCOs generated from multiple iPSC lines, demonstrating the robustness of this protocol (Table S1). Furthermore, the expressions of CD16, CD14, and CD11b in HCO immune cells were confirmed by cytometry by time of flight (CyTOF) analysis. In CyTOF analysis, CD45+ hematopoietic cells made up 1.5%–2.5% of the viable cells in day 35–day 42 HCO cultures (Figure S5A). Of the CD45+ cells, 5%, 11%, 41%, and 16% were labeled with high CD11b, CD16+, CD14+, and CD16+CD14+, respectively (Figures S5B–S5E). RNA-seq confirmed the expression of all the above markers and *TIMD4*, *LYVE1*, *FOLR2*, *HLA-DRA*, *ITGAX*, and *ADAMDEC1* (Figures 3E, 4A, and 5C). Moreover, day 37 HCO macrophages expressed markers associated with both murine self-maintaining lamina propria macrophages[7] and broad tissue-resident macrophages[10] (Figures 5D and 5E). Specifically, HCO macrophages expressed markers associated with long-lived macrophages that are associated with enteric neurons and blood vessels. In addition, HCO macrophages expressed markers associated with TIMD4+LYVE1+FOLR2+ (TLF+) and MHC-II macrophage subtypes. Markers associated with gut-associated lymphoid tissue, Paneth cells, and more transient CCR2 macrophages were less enriched.

Next, we performed flow cytometry analysis of HCO macrophages and found that approximately 2% of viable cells in HCOs were positive for monocyte/macrophage marker CD64/FCGR1A (Figures 5F, 5G, and S5F). We then gated the flow data based on the co-expression of two published markers known to distinguish tissue-resident macrophage subpopulations in multiple tissues.[10] We found that 5%, 89%, and 65% of the CD64+ cells expressed CD192/CCR2, CD14, and TIMD4, respectively (Figures 4H, 4I, and S5G). The scRNA-seq data confirmed that markers of distinct TLF+, MHC-II, and CCR2-like macrophage subtypes were expressed in day 37 HCO and fetal colon macrophages (Figures 4J and 4K). These results support the conclusion that HCOs contain TLF+ and MHC-II long-lived tissue-resident macrophages that resemble human fetal colon macrophages.

To determine whether macrophages in HCO cultures acquire a transcriptional signature resembling human fetal colon macrophages and whether they are distinct, we compared them with macrophages from other fetal organs.[15] This comparison revealed them to be transcriptionally distinct (Figures 3K and 5A). We then compared HCO hematopoietic cells with those from more closely related endoderm organs (Figures 5B–5D), including the fetal colon, small intestine, stomach, esophagus, lung, and liver isolated from human fetuses between 7 and 21 weeks post-conception.[57] The day 37 HCO hematopoietic cells were primarily composed of monocyte/macrophage lineages, and Pearson correlation revealed that they most closely resembled those of the fetal GI tract (Figures 5C–5E). We then focused on myeloid lineages using the reference Yu et al.[57] fetal monocyte/macrophage atlas. Although immature day 22 myeloid cells mapped to small intestine, lung, and stomach, HCO macrophages at later stages (day 28 and day 37) began to resemble fetal intestinal and colonic macrophages (Figure 5F). We identified an organ-enriched gene signature in fetal tissue-resident macrophages (Figures 5A and 5G) and used ensemble clustering to deduce the relationship between HCO macrophages and those in other

human fetal organs. We confirmed that day 37 HCO macrophages acquired an expression signature resembling macrophages in the small intestine and colon (Figures 5H and 5I). Monocytes/macrophages derived directly from hPSCs did not acquire this GI macrophage transcriptional signature (Figures 5A and 5F–5I). Clustering analysis revealed that the day 37 HCO immune cells overlapped with the fetal monocyte/macrophage atlas (Figure 5J). The relative proportion of HCO cells in each cluster mirrored the fetal colon, particularly *ATOX1* and *FUCA1* clusters, which are predominately in mid/HG macrophages (Figures 5K and 5L). Relatively no HCO macrophages mapped to lung-specific cluster 8, but some did cluster with liver-specific macrophages. These data provide evidence that macrophages that co-develop within HCO cultures *in vitro* acquire a tissue-resident transcriptional signature resembling their *in vivo* counterparts.

## HCO macrophages responded to anti- and pro-inflammatory signals

Gene ontology (GO) analysis of bulk RNA-seq and scRNA-seq revealed that by day 37, a subset of HCO macrophages expressed inflammatory cytokines, including interleukin (*IL*)-*8*, *CCL3*, and *CCL4* (Figures 6A and S1C). According to the scRNA-seq data, the mRNAs for these pro-inflammatory cytokines and other inflammatory mediators were produced almost exclusively by the myeloid cells within the culture and not by epithelial or mesenchymal cells (Figure 6A). The expression of several pro-inflammatory cytokines and chemokines was higher in the macrophages from HCOs than in the macrophages in fetal colon, suggesting that the macrophages within HCOs exhibit a basal level of inflammation *in vitro* (Figure 6B). Luminex multiplexed ELISAs confirmed that HCOs secreted significantly higher levels of the pro-inflammatory cytokines IL-6, IL-8, CCL3, and CCL4 than HIOs (Figure 6C). The secretion of these pro-inflammatory cytokines could be inhibited by the addition of the inflammation-suppressing cytokine IL-10 (Figure 6D),[63–65] indicating that mechanisms of *in vivo* IL-10-mediated immune tolerance[66–69] are conserved in HCO cultures.

To confirm that macrophages were the source of inflammation in HCO cultures, we used a modified HCO culture protocol that restricts immune cell co-development[70] (referred to as HCO [mod]) (Figures S6A and S6B). Principal-component analysis (PCA) and GO analysis of differentially expressed genes revealed that HCO (mod) lacked the immune cell and inflammatory signature observed in standard HCOs (Figures S6C and S6D). Importantly, HCOs lacking immune cells had a normal colonic phenotype suggesting that macrophages are not required for HCO development. We also depleted macrophages starting at a later stage of HCO development (day 35) using an anti-M-CSF anti-body (Figures S6F and S6G). Macrophage depletion did not affect organoid integrity as evidenced by the maintenance of epithelial structure. However, macrophage-depleted HCOs had reduced expression of cytokines compared with vehicle control HCOs (Figure S6H). Collectively, these results indicate that the macrophages were the source of pro-inflammatory cytokines and that the depletion of immune cells did not grossly alter HCO patterning and development.

We next determined if HCO macrophages behave like fetal tissue-resident macrophages, which mount an inflammatory response to lipopolysaccharide (LPS) stimulation.[71] HCO macrophages express the components of the receptor complex that mediates the

inflammatory response to LPS including *TLR4*, *CD14*, and *LY96* (Figure 6A).[72,73] Treatment of HCOs with LPS significantly increased IL-6, IL-8, CCL3, CCL4, and TNF-a secretion (Figures 6E and S6H). This cytokine response to LPS was mostly attenuated with macrophage depletion using an anti-M-CSF antibody (Figure S6H). In addition, treatment of HCOs with LPS rapidly triggered macrophage motility and chemotaxis toward foci within the organoid (Figure 6F; Video S2). To determine whether LPS stimulation could induce epithelial cell death in HCOs, we treated HCOs and HIOs with a high concentration of LPS (500 ng/mL) which resulted in severe necrosis of organoids at 1 h post LPS addition, based on live imaging using SYTOX dead cell stain (Figure 6G; Video S3). In contrast, HIOs were largely resistant to LPS-triggered cell death. Collectively, these data indicate that HCO-associated macrophages can mount a rapid and robust inflammatory response to LPS resulting in epithelial necrosis.

## HCO macrophages phagocytose bacteria and respond to commensal and pathogenic bacteria in the lumen

Macrophages phagocytose bacteria,[74] a process that is mediated in part by scavenger receptors, Fcg receptors, and complement receptors.[75] Analysis of scRNA-seq data revealed that subsets of these receptors are expressed on HCO macrophages (Figure 6A). To examine the phagocytic function of HCO macrophages, we treated HCOs with *E. coli* particles labeled with a pH-sensitive fluorophore. Live imaging revealed that HCO macrophages continuously extend filopodia and survey the microenvironment (Video S4). HCO macrophages phagocytosed bacterial particles within acidic phagolysosomes, as evident by the increase in pH-sensitive fluorescence (Figures 6H and 6I). Furthermore, microinjection of live commensal or pathogenic enterohemorrhagic *E. coli* (EHEC) resulted in macrophage migration toward the epithelium or in some cases into the lumen of HCOs with significantly less luminal migration in commensal versus pathogenic *E. coli* (Figures 6J and 6K). Pathogenic bacteria such as EHEC and salmonella can disrupt epithelial barrier integrity, allowing the transmigration of macrophages.[76] Collectively, our data indicate that macrophages from HCOs are functional resident-like macrophages capable of responding to bacterial particles and live bacteria.

## HCO macrophages establish residency and are not displaced by bone-marrow-derived macrophages

Since HCO macrophages acquired a transcriptional signature reminiscent of colon tissue-resident macrophages (Figures 5B–5L), we investigated whether they continued to maintain residency during long-term HCO development. To extend the development of HIOs and HCOs, we transplanted them for an additional 4 months[36,77,78] (Figure 7A). Transplanted (TXP) HIOs and HCOs resemble the human fetal small intestine and colon both histologically and transcriptionally[36] (Figures 7A and S7A–S7I). We next determined whether the human tissue-resident macrophages (hCD163+) were maintained within the organoid tissue or were replaced by host-derived murine macrophages (F4/80) (Figure 7B). HIOs TXPs did not contain any human CD163+ macrophages but had abundant mouse F4/80+ macrophages in the lamina propria and throughout the villi (Figures 7C–7E). By contrast, HCO TXPs had abundant CD163+ macrophages that were much more prevalent than host-derived F4/80 macrophages (Figures 7C, 7D, and S7A). The CD163+

macrophages were predominantly located in the lamina propria but could also be detected in the submucosa and muscularis layers of the graft (Figures 7C–7E and S7A). In the muscularis layers, the CD163+ cells were interspersed with F4/80+ cells, suggesting that both tissue-resident and circulating macrophages could colonize these tissue layers. scRNA-seq of 15-week HCO TXPs confirmed that colonic epithelium contained the same cell types as seen histologically. The number of macrophages detected by scRNA-seq was lower than expected based on histology (Figures S7A–S7G), likely due to technical reasons. Examination of blood and bone marrow from HCO TXP mice revealed that they do not contain human CD45+ cells, supporting the notion that immune cells from the HCO graft did not colonize the bone marrow (Figure 7F). These data indicate that HCOs can generate self-maintaining macrophages that are not derived from HSCs.

## DISCUSSION

Lineage-tracing experiments in mice show that except for microglia, all hematopoietic cells that persist in the embryo are derived from HE present at various sites of the embryo including yolk sac and AGM. Here, we show that BMP signaling required to promote HCO patterning also promotes the formation of HE-like cells in HCOs as previously shown in studies of the HE transcription factor GATA2.[35,46,79] Comparison of scRNA-seq datasets suggested that HCO hematopoietic cells are transcriptionally similar to those derived in 2$^{nd}$ wave hematopoiesis in the fetal yolk sac and AGM. In mice, lineage tracing and embryo microdissection would allow for the identification of the tissue sources of hematopoietic cells, but similar approaches are difficult in human organoid cultures. Therefore, further delineation of hematopoietic cell ontogeny in organoids will require the development of lineage-tracing tools.

Our data suggest that the HCO environment provides the cues necessary for the development of multipotent EMPs, with transcriptional evidence supporting the presence of multipotent HPCs and lymphoid progenitors. The presence of these progenitors was transient, as endogenous factors within the cultures, including CSF1, promoted robust myeloid differentiation from HPC-like cells to GMP to myeloblast to finally monocytes and macrophages that persist in passaged HCOs. This is distinct from a previous study of co-developing macrophages/microglia in cerebral organoids, which originated directly from brachyury+ mesodermal cells reminiscent of primitive hematopoiesis.[80] Furthermore, the co-development of macrophages within the HCO *in vitro* microenvironment promoted them to acquire transcriptional signatures reflecting human fetal intestinal/colonic tissue-resident macrophages.[10,57] Moreover, HCO macrophages were not displaced by the host bone-marrow-derived macrophages following transplantation. These organoid data suggest the possibility that, like in mice, human tissue-resident macrophages of the intestinal tract could have a fetal origin and/or the tissue is able to confer regional specificity to the macrophages.

Macrophages function in the development of the brain,[81] bone,[82] and mammary gland.[83] However, few studies have examined their role in GI tract development. Our results indicate that HCOs could pattern and grow normally in HCO cultures where macrophages were absent or depleted. Csf1r null mice, which have decreased numbers of tissue-resident

macrophages,[84] were reported to have shorter colonic crypts and increased goblet cell numbers at the expense of enteroendocrine cells at postnatal day 14.[85] However, it is unclear whether this effect is due to altered *in utero* development or response to colonization by commensal bacteria since fetal mice were not examined. Similar studies could be conducted on TXP HCOs derived from CSF1R-deficient or CSF1-deficient hPSCs. Additionally, HCO-culture-derived monocytes/macrophages could be introduced into other GI organoid systems (which currently lack them) to examine the effect of macrophages on organoid development as well as the effect of regional identity on the acquisition of a tissue-specific resident macrophage signature.

The derivation of HCOs with resident macrophages provides a new tool for examining the interaction between innate immune cells and the colonic epithelium. In addition, HCOs could be used to determine the niche factors that allow the maintenance of tissue-resident macrophages. HCOs should allow the modeling of inflammatory diseases such as necrotizing enterocolitis; very early onset IBDs[86]; bacterial pathogens such as *Clostridium difficile*; and viral pathogens such as HIV, which readily infects fetal intestinal macrophages.[87] In addition, the incorporation of other immune cell types could be used to study other innate immune mechanisms such as neutrophil-driven inflammatory hypoxia.[88] Lastly, this study provides a framework for the generation of other human organoid systems containing resident immune cells.

## Limitations of the study

Although HCOs give rise to EMPs, the presence of multipotent HPCs with lymphoid potential is based on transcriptional comparisons and not functionally validated. Furthermore, we do not know whether HCO cultures contain yolk sac and, therefore, cannot rule out yolk sac as a source of these progenitors. The progenitors in cultures quickly lose multipotency and differentiate toward the myeloid lineage. This occurs without exogenous perturbations; therefore, it is difficult to maintain the MPP pool. Temporal growth factor manipulations would likely be required to generate and maintain stable hematopoietic and lymphocyte progenitor populations. Overcoming these difficulties will be critical for the accurate modeling of complex diseases such as IBDs, which involve both innate and adaptive immune cells.

Our scRNA-seq studies provide significant insights into the development of multiple cell types in HCO cultures. However, scRNA-seq is highly dependent on tissue dissociation, and HCOs with dense mesenchyme, especially TXPs, are technically difficult to dissociate. We and others have shown that most single-cell isolation approaches for GI tissues result in the loss of mesenchyme[57] and other submucosal cells, including enteric neuroglia cells.[89] Cell types and relative proportions of cells, particularly colonic epithelium and mesenchyme, are underrepresented in our *in vitro* datasets, missing aspects of cellular complexity and cell-cell interactions occurring within HCO cultures.

# STAR★METHODS

## RESOURCE AVAILABILITY

**Lead contact—**For additional information and requests for resources, reagents, or codes, please contact Jorge Múnera (munera@musc.edu).

**Materials availability—**All human induced pluripotent stem cells lines, including wild-type and CDX2 CRISPR/Cas9 null, generated in the study are available upon request with appropriate MTA. New lines are listed in the key resources table.

### Data and code availability

- Bulk RNA-seq and scRNA-seq datasets generated in this study are publicly available in NCBI's Gene Expression Omnibus (GEO): GSE240363. All accession numbers used in this study are listed in the key resources table.
- All scRNA-seq analysis was performed in R using previously generated codes, which are referenced in the key resource table. This paper does not report original code.
- Additional information, original images, digital scans of cytospins, or scripts needed for further analysis are available upon request.

## EXPERIMENTAL MODELS

**Human PSC Line Generation and Maintenance—**All human ESC (H1, WiCell, RRID: CVCL_9771) and control iPSC lines, including 72.3 (RRID: CVCL_A1BW), 115.3 (RRID: CVCL_C1U9), 209.2, and 263.10 were obtained from the Cincinnati Children's Hospital Medical Center (CCHMC) Pluripotent Stem Cell Facility. Human iPSC lines were generated from either foreskin fibroblasts using episomal plasmids (72.3, 115.3) or peripheral blood mononuclear cells using lentiviral transduction (209.2, 263.10) as previously described.[35,90] All lines were derived from male donors with the exception of 209.2, which was female. HPSCs were maintained in mTeSR1 (StemCell Technologies) on hESC-qualified Matrigel (Corning) coated Nunclon Delta Surface 6-well plates (Thermo Scientific). Spontaneous differentiation was manually removed and cells were passaged every 3–4 days using Dispase. Cells were routinely confirmed to be karyotypic normal and mycoplasma negative.

**Animals—**Immune-deficient NOD-SCID IL-2Rγgnull (NSG) mice, 8–16 weeks old, were used in transplantation experiments (obtained from the Comprehensive Mouse and Cancer Core Facility, Cincinnati, Ohio). Wild type mice were used for studies on fetal mice. All mice were housed in the animal facility at CCHMC. Both sexes were utilized for studies. All experiments were performed with the approval of the Institutional Animal Care and Use Committee of CCHMC.

## METHOD DETAILS

**Directed Differentiation of human PSCs into HIO, HCOs, and Macrophages—**Generation of HIOs and HCOs has been previously published.[36,37] Briefly, human ES

and iPSCs were plated as single cells in mTeSR1 media plus ROCK inhibitor Y27632 (10 μM; Stemgent) on hESC-qualified Matrigel (Corning)-coated 24-well plate at 150,000 cells per well. Beginning the next day, cells were treated with Activin A (100 ng/ml; Cell Guidance Systems) for three days in RPMI 1640 (Invitrogen) containing increasing concentrations of 0%, 0.2%, and 2.0% define fetal bovine serum (dFBS; Invitrogen). For endoderm induction of iPSC72.3, BMP4 (15 ng/ml) was added to the first day of Activin A treatment. Following definitive endoderm induction, cells were treated for 4 days with FGF4 (500 ng/ml; R&D Systems) and CHIR99021 (3 μM; Stemgent) in RPMI 1640 with 2.0% dFBS to generate 3-dimensional mid-hindgut spheroids. Alternatively, HIO or HCO (mod) were generated by the force aggregation of mid/hindgut monolayer clumps as previously described.[70] These mid/hindgut spheroids or aggregates were embedded in basement-membrane Matrigel (BD Biosciences) and subsequently grown in Advanced DMEM/F12 (Invitrogen) supplemented with N2 (Invitrogen), B27 (Invitrogen), L-glutamine, 10 μM HEPES, penicillin/streptomycin, and EGF (100 ng/ml; R&D Systems). Organoids were densely plated (>50 per bubble) in Matrigel for first two weeks to promote endothelial tube and hematopoietic cell generation. For proximal HIO and HCO specification, Noggin (100 ng/ml; R&D Systems) or BMP2 (100 ng/ml; R&D Systems) was added for the first three days of three-dimensional growth, respectively. Organoids were transferred to new Matrigel following 2–3 weeks.

For generation of monocyte/macrophages from hPSCs, hematopoietic progenitors were generated using STEMdiff™ Hematopoietic Kit (StemCell Technologies) according to manufacturer's instructions. Briefly, H1s were dissociated into single cells in mTeSR1 with ROCK inhibitor and plated into anti-adherence treated AggreWell 400 (StemCell Technologies) 24-well plates. After 48 hrs, embryoid bodies were moved to Matrigel coated 12 well plate and incubated in mTeSR overnight. Cells were cultured in basal medium supplemented with Medium A for 3 days followed by Medium B for 9 days. HPCs were collected, moved to 6 wells plate, and maintained in DMEM/F12 supplemented with 10% dFBS, 1% penicillin/streptomycin, 10 ng/mL GM-CSF (R&D Systems), and 25 ng/mL M-CSF (R&D Systems) for 14 days to differentiate into monocyte/macrophages.

**Transplantation of human intestinal and colonic organoids—**NSG mice were kept on antibiotic chow (275 p.p.m. Sulfamethoxazole and 1,365 p.p.m. Trimethoprim; Test Diet). Food and water was provided *ad libitum* before and after surgeries. A single HIO or HCO, matured *in vitro* for 35 days, was removed from Matrigel, washed with cold phosphate-buffered saline (DPBS; Gibco), and transplanted under the kidney capsule as previously reported.[78] Briefly, the mice were anesthetized with 2% inhaled isoflurane (Butler Schein), and the left side of the mouse was then prepped in sterile fashion with isopropyl alcohol and povidine-iodine. A small left-posterior subcostal incision was made to expose the kidney. A subcapsular pocket was created and the organoid was then placed into the pocket. The kidney was then returned to the peritoneal cavity and the mice were given an IP flush of Zosyn (100 mg/kg; Pfizer Inc.). The skin was closed in a double layer and the mice were given a subcutaneous injection with Buprenex (0.05 mg/kg; Midwest Veterinary Supply). At 8–15 weeks following engraftment, the mice were then humanely euthanized or subjected to further experimentation.

**Generation of CDX2 knockout iPSC line—**CRISPR/Cas9 was used to knockout the endogenous CDX2 gene by introducing biallelic indel mutations. Guide RNAs (gRNA) were designed according to the on- and off- target scores from web too (http://CRISPOR.org). Pairs of complementary oligos containing gRNA target sequence (g508: GTCGCTACATCACCATCCGG) with overhangs were cloned into modified pX458 vector that carries an optimized sgRNA scaffold and a high-fidelity eSpCas9(1.1)-2A-GFP.[97,98] High editing activity was validated in HEK293T cells by the T7E1 assay. To generate CDX2 knockout iPSCs, 1.8E6 cells were reverse transfected in 2 ml of mTeSR1 with 4 μg of g508 plasmid using TransIT-LT1 (Mirus). Starting two hours post-transfection, cells were fed daily with MEF-conditioned media containing 10 μg/ml bFGF. At 72 hr post-transfection, single GFP+ cells were isolated using FACS and plated at cloning density in 6-well plates coated with 0.1% gelatin and 1.87E5 irradiated CF1-MEF feeders per well. Plates were fed daily with MEF-conditioned media with 10 ng/ml bFGF. Single clones were manually excised, transferred to hESC-qualified Matrigel-coated 24-well plates containing mTeSR1 for expansion and subjected to genotyping to confirm biallelic frameshift mutation. Parental iPSC 115.3 was used as CDX2 wildtype control.

**Tissue processing, immunofluorescence, and microscopy—**Tissues were fixed for 1–24 hr in 4% paraformaldehyde (PFA) on ice depending on the size of the fixed tissue. Organoids and transplant engraftments were frozen in OCT. OCT sections were blocked using donkey serum (5% serum in 13 PBS plus 0.5% Triton-X) for 30 min and incubated with primary antibody overnight at 4 °C. Slides were then washed 3X with 1X PBS plus 0.5% Triton-X and incubated in secondary antibody with DAPI in blocking buffer for 2 hr at room temperature (23°C). Please see key resources table for list of antibodies and respective dilutions. Slides were then washed 2X with 1X PBS plus 0.5% Triton-X followed by a final wash in 1X PBS. Slides were then mounted using Fluoromount-G® (SouthernBiotech). Images were captured on a Nikon A1 confocal microscope (CCHMC) or a Zeiss LSM 880 NLO confocal microscope (MUSC) and analyzed using NIS Elements (Nikon) or Imaris Imaging Software (Bitplane). For whole-mount staining, tissues were processed similarly as above and then dehydrated with methanol and cleared in Murray's solution (benzyl alcohol: benzyl benzoate; 1:2). Imaging was performed with a Nikon A1 confocal microscope or a Zeiss LSM 880 NLO confocal microscope.

**RNA isolation and RT-qPCR—**RNA was extracted using NucleoSpin® RNA extraction kit (Macharey-Nagel) according to manufacturer's protocols. For cDNA reverse transcription, the Superscript VILO (Invitrogen) was used to synthesize cDNA. RT-qPCR primers were designed using the qPrimerDepot web-based tool (primerdepot.nci.nih.gov). Primer sequences are listed in Table S2. RT-qPCR was performed using Quantitect SYBR® Green PCR kit (Qiagen) and a QuantStudio™ 6 Flex Real-Time PCR System (Applied Biosystems). Relative expression was determined by ΔΔCt and data were normalized to control samples. *PPIA* was used as housekeeping gene.

**Bulk RNA-seq sequence assembly abundance estimation—**RNA library construction and RNA sequencing was performed by the CCHMC DNA Sequencing Core, using an Illumina HiSeq2500 platform or by BGI using the DNBseq platform. The quality

of the Illumina sequencing runs was evaluated by analyzing FASTQ data for each sample using FastQC version 0.10.1(http://www.bioinformatics.babraham.ac.uk/projects/fastqc) to identify features of the data that may indicate quality problems (e.g. low quality scores, over-represented sequences, inappropriate GC content, etc.). No major issues were identified by the QC analysis. We used the software package Tuxedo Suite for alignment, differential expression analysis, and post-analysis diagnostics. Briefly, we aligned reads to the reference transcriptome (UCSC hg19 for H1 HIO and HCO or hg38 for HIO mod and HCO mod) using TopHat version 2.0.13 and Bowtie version 2.2.5.[91,92] We used default parameter settings for alignment, with the exception of: "–b2-very-sensitive" to maximize the accuracy of the read alignment, as well as "–no-coverage-search" and "–no-novel-juncs" limiting the read mapping to known transcripts. Cufflinks version 2.2.1[92] was used for RNA abundance estimation. UCSC hg19.fa was used as the reference genome sequence and UCSC hg19.gtf was used for transcriptome annotation. We applied the following parameters in Cufflinks: "–multi-read-correct" to adjust expression calculations for reads that map in more than one locus, and "–compatible-hits-norm" and "–upper-quartile –norm" for normalization of expression values. Normalized TPM tables were generated using the CuffNorm function. RNA sequence assembly and transcriptional analysis was conducted using the 64-bit Debian Linux stable version 7.10 ("Wheezy") platform. Similar QC analysis was performed with data from the DNBseq platform and downstream analysis was performed using Partek® Flow® software. Heatmaps are represented as $\log_2$ transformed TPM+1. HIOs and HCOs are from three-four independent differentiations.

**Tissue Dissociation for Single Cell RNA-seq—**Dissociation of 22- and 37-day old *in vitro* HCOs and 15 wk HCO TXPs were performed using slightly modified published protocols.[57,99] Briefly, *in vitro* HCOs from 2–3 wells were pooled and pretreated with ice cold PBS and Cell Recovery Solution (Corning) to remove Matrigel. HCO TXPs were opened removed of mucus and outer muscle layer and a piece was removed for dissociation. Organoids were finely minced using a scalpel in ice cold HBSS with $Mg^{2+}$ and $Ca^{2+}$. Original supernatants were spun down at 1,300 rpm and added to minced tissue. All tubes and tips were coated with 1% BSA. Minced *in vitro* HCOs were enzymatically dissociated using enzymes from the Neural Tissue Dissociation Kit (Miltenyi Biotec) prepared and added using manufacturer's protocol or TryPLE for HCO TXP and incubated at 37°C or 4°C, respectively. Organoids were incubated for approximately 60 min with periodic shaking and fluxing through P1000 and P200 pipette tip. For 28-day old HCO immune cell collection, cells suspended in the media overlaying Matrigel were collected without enzymatic digestion. All dissociated cells were filtered through BSA coated 70 μm and 40 μm cell strainers to remove undissociated tissues. A single cell suspension with >80% viability was confirmed using a hemocytometer. Two individual replicates from d22 HCO were collected from different wells of the same differentiation and kept separate through dissociation process. The d22, d28, d37, and 15 wk TXP HCO datasets were all from distinct differentiations. Monocytes/macrophage separately derived from iPSCs were removed from 6 well plate using short Trypsin-EDTA (ThermoFisher) treatment and then exposed to same mechanical, temperature, and enzymatic perturbations as dissociating *in vitro* HCOs.

**Single Cell RNA-seq, Alignment and Analysis—**Single cell RNA-Seq library preparation for *in vitro* HCOs was performed by the CCHMC Gene Expression Core using the Chromium 3'v2 for d28 HCO and 3'v3 GEM Kit for other conditions (10x Genomics). Approximately 8,700 or 12,800 cells were loaded to achieve 5,000 or 8,000 captured cells per d28 HCO or all other samples to be sequenced, respectively. Sequencing was performed by the CCHMC DNA Sequencing core using the HiSeq 2500 or NovaSeq 6000 (Illumina) sequencing platform with an S2 or S4 flow cell to obtain approximately 320 million reads per sample. Raw scRNA-seq data was converted to FASTQ files and then aligned to the human genome [hg19 d28 HCO, d37 HCO, HCO TXP or hg38 for d22 HCO, d14 macrophages] using CellRanger v3.0.2 (10x Genomics). All human fetal reference datasets were either kindly provided by the Spence or Camp laboratories[57] or available on GitHub and/or Gene Expression Omnibus repository (GSE162950, GSE133345). Individual analysis, including quality controls and clustering, of all datasets was first performed using Seurat [v3.2.3][93] in R [v3.6.3] unless otherwise noted. Basic filtering parameters for gene detection included greater than or equal to 3 cells and all cells with minimum 100 detected genes and maximum 7,500 genes. Percent.mito parameter was all cells less than 20. Data was normalized using SCTransform in Seurat. Cell cycle effect was regressed out using previously established methods in Seurat. Normalized expression levels underwent principal component analysis (PCA) followed by uniform manifold approximation and projection (UMAP)[100] with subsequent Louvain clustering. Cluster resolution was changed to increase or decrease number of clusters identified. Datasets from two independent d22 HCO replicates were merged together using Seurat prior to normalization, PCA, UMAP, and clustering. Marker genes were determined using 'FindAllMarkers' function (Wilcoxon rank-sum test). Clusters were annotated manually by differential marker expression in individual Seurat clusters or using unbiased methods. For instance, 'MapQuery' was utilized to transfer integration anchors and annotations from a reference dataset onto query datasets using Seurat [v4.2.1]. Alternatively, we utilized an 'Ensemble learning for harmonization and annotation of single cells' ('ELeFHAnt') package, which predicted cell-type annotations based on reference metadata used as a training dataset (Thorner et al. (2021). BioRxiv). Cell annotation of the query dataset was based on reference dataset metadata. Cell proportions were determined by cell counts in each Seurat cluster normalized to total number of cells. After data scaled and normalized in Seurat, feature plots and dot plots were generated using 'ggplot2' in Seurat. Genes were manually selected, differentially expressed, or from published datasets as noted. Signaling inference was performed using 'CellChat' in Seurat [v4.1.1] to identify expressed ligands and receptors in individual Seurat clusters to predict relevant cross cluster signaling.

After individual dataset analysis, we integrated all cells from different HCO time points and/or human fetal datasets together using basic integration vignette in Seurat[101] using 2,000 integration features. For all integration analysis, normalized levels underwent PCA followed by UMAP and Louvain clustering and annotated using similar methods to individual samples. To analyze different cell populations, including mesenchyme, hematopoietic cells, HPCs, and/or monocyte/macrophages from integrated datasets, we identified the Seurat clusters expressing cell population-specific markers and subsetted and re-clustered using 2,000 integration features, normalized and underwent PCA and UMAP

and Louvain clustering. In the analysis of monocyte/macrophage cell data from d37 HCO compared to fetal endodermal atlas, we first subsetted the monocyte/macrophages cells identified from each individual sample. Then, similar to our integration for all cells, we performed Seurat Integration for all monocyte/macrophage samples and used the human fetal endodermal organ monocyte/macrophages as the reference dataset. Cell proportions were compared between datasets. Following normalization and scaling, RNA expression from different datasets was compared using dot plots, positive Pearson and Spearman correlations using 'corrplot', or by similarity score predicted using deduce relationship function of EleFHAnt. More specifically, 'EleFHAnt' uses expressional reference dataset to train both 'RandomForest' and 'Support vector machines' (SVM) classifiers to assign a similarity score to query dataset cells. Ensemble is a combination of both 'RandomForest' and 'SVM' classifiers. Psuedotime trajectory was performed using 'Monocle3'. The origin node was selected based on expression of CD34 and other early known HPC markers and no distinct branch points were predicted.

**Hemogenic Endothelium Assay—**HCOs were dissociated into single cells and CD34+ cells were isolated by magnetic-activated cell sorting (MACS) using the human CD34 Microbead Kit (Miltenyi, 130046702). CD34+ cells were then plated 24-well plates coated with Matrigel and EHT assay was performed using a modified version of a published protocol.[102] Briefly, CD34+ cells were cultured in StemPro-34 media (Gibco, 10639011) supplemented with BMP4 (10ng/ml, day 0–2), bFGF (5ng/ml), VEGF (5ng/ml), SCF (100ng/ml), EPO (2 U/ml), IL-6 (10ng/ml), IL-11 (5ng/ml), TPO (30ng/ml), Flt-3L (10ng/mL), IGF-1 (25ng/ml), SHH (20ng/ml), Angiotensin II (10μg/ml) and Losartan (100μM) for 5 days with media changes every 2–3 days. After 5 days, floating cells were analyzed for CD34 and CD45 expression using flow cytometry.

**Flow cytometry of HCOs—**Organoids were washed in ice cold PBS to dissolve Matrigel. Organoids were then mechanically minced with a scalpel and digested in TrypLE with 10 uM ROCK inhibitor at 37°C for 60–90 min with vigorous shaking every 10 min until tissue was homogenized. An equal vol. of DMEM + 10% FBS media was added to the homogenized mixture and filtered through a 100μm membrane. The filter containing un-dissociated tissues were further digested with 2mL Accutase at 37°C for 10 minutes and contents washed with DMEM + 10% FBS media. The cell mixture was then centrifuged at 500xg for 5 minutes and pellet was resuspended in staining buffer (2% FBS in PBS supplemented with 10 uM DNAse and 10 uM ROCK inhibitors). After Fc block, cells were incubated with fluorophore-conjugated antibodies in the dark for 30 minutes. A list of antibodies is provided in the key resources table. Flow cytometry was performed on up to 100,000 cells using a Beckman Coulter CytoFLEX LX machine and the data was analyzed using FlowJo software. Side scatter (SSC) and forward scatter (FSC) were used to gate for cells, FSC (height) and FSC (area) were used to gate for single cells. Live-or-Dye kit (32009-T, Biotium) was used to negatively identify live cells as per the manufacturer's protocol.

**CyTOF—**For CyTOF analysis was performed as previously reported.[103] Briefly, 16–20 HCOs ranging from d35-d45 were pooled for one experiment and experiment was

performed twice. Following dissociation into single cells, cells were processed according to manufacturer's instructions (Fluidigm). This included being pretreated with Cisplatin, fixed, permeabilized, barcoded, and stained with hematopoietic-specific cell surface antibodies conjugated with elemental isotopes according to manufacturer's instructions. A list of antibodies is provided in the key resources table. Cells were fixed, intercalated, and shipped to the University of Rochester's Cytometry Research Core Facility where they were subjected to CyTOF/mass cytometry on a Helios (Fluidigm).

**Cytospins—**Cells were cytospun at 500 rpm for 5 min and stained with Differential Quik modified Giemsa (Electron Microscopy Sciences) according to manufacturer's protocol. Briefly, Cytospun slides were dipped 20 seconds in fixative solution (solution A), followed by multiple dips for 30 sec in solution C-Red and 5 dips in solution B-Blue. Slides were rinsed several times in distilled water (until water is clear) and air dried for 1 hr. Finally, slides were dipped in xylene 4 times and mounted with Cytoseal 60 (ThermoFisher Scientific) and cover-slipped. Entire slides were imaged digitally using ScanScope and images available upon request.

**Methocult™ assays—**Methocult™ assays were run according to the manufacturer's protocol. Briefly 10,000 to 40,000 cells were resuspended in Methocult™ medium and plated in a 6 well dish. The dish was then incubated for 2–3 weeks to allow the formation of colonies. Colonies were then counted, scored based on morphology, and collected for RNA analysis.

**LPS or IL-10 stimulation and Luminex Array—**HCOs were grown for 35 days and then treated overnight with 100 ng/ml of Ultrapure lipopolysaccharide from *E. coli* K12 (Invitrogen) or treated for 7 days with 50 ng/ml of rhIL-10 (R&D Biosystems). Water was used as a vehicle control for addition of LPS or rhIL-10. For Luminex arrays, supernatants from HIO and HCO cultures were collected and sent to the CCHMC Research Flow Cytometry core which processed and analyzed the samples according to the manufacturer's protocol.

**Depletion of macrophages with MCSF antibody—**For MCSF antibody-mediated macrophage depletions, 35 day old HCOs were treated with 500 ng/ml of MCSF neutralizing antibody for 7 days and then subjected to LPS stimulation and Luminex arrays as detailed above.

**Live imaging of *E. coli* particle phagocytosis—**For live imaging 35–45 day old HCOs were replated in an Ibidi 2 well chamber. Minimal Matrigel was used to prevent antibodies from "sticking" to Matrigel. Organoids were then incubated in basic gut media with EGF and containing CD14 Monoclonal Antibody (TuK4), FITC (MHCD1401 Thermofisher) and placed back in incubator for ~6 hours to allow binding of antibodies to the surface of macrophages. The media was then replaced with fresh media basic gut media with EGF ± pHrodo™ Green *E. coli* BioParticles™ (Thermofisher). Ibidi 2 well chambers were then placed in a live imaging chamber set to 37°C and 5% $CO_2$. Several fields per well were then imaged at 2 min intervals for 3 hr using a Nikon A1R confocal. For quantification of E. coli particle phagocytosis, organoids were cultured overnight and

phagocytosis was quantified by quantifying the relative pixels of CD14 to the relative pixels of green fluorescence from the pHrodo™ Green *E. coli* BioParticles™ using Imaris Imaging Software (Bitplane).

**Microinjection of bacteria—**Drummond glass capillaries (Fisher, cat. 21–171–4) were pulled with a micropipette puller (Sutter Instrument Company). The sealed tips of the capillaries were then cut open using Cuterz glass scissors, and capillaries were then loaded onto Nanoject II auto-nanoliter injector (Fisher, cat. 13–681–455). Microinjections were performed with images being taken before and after injection using a stereo-microscope (Leica). To ensure proper injection, 2.5 mg/ml FITC was co-injected to visualize the HCO lumen. The HCOs were then incubated in a tissue culture incubator at 37°C with 5% $CO_2$ for 5 hr. For bacterial infections, approximately $10^3$ *E. coli* cells were microinjected into the HCO lumen with PBS injection serving as a negative vehicle control. The HCOs infected with *E. coli* were then incubated in basic gut media containing antibiotics at 37°C in a humidified chamber with 5% $CO_2$ overnight.

### QUANTIFICATION AND STATISTICAL ANALYSIS

For animal experiments such as those in Figures 1 and S1, “n” represents the number of animals which were analyzed. For experiments involving patterned spheroids and *in vitro* grown organoids, “n” represents the number of biological replicates (2–3 wells were collected for each replicate). For experiments involving transplanted organoids, “n” represents the number of individual animals that were transplanted with a single organoid. Quantification of data are represented as mean ± SD unless otherwise specified. Significance was determined by either unpaired t tests with 2-tailed distribution and two-sample equal variance when comparing 2 conditions or one-way ANOVA with Tukey’s multiple comparison test when comparisons >2 conditions. Significance represented as $p<0.05$*, $<0.01$**, $p<0.001$*** as denoted in Figure legends. Statistics were performed and graphs were generated in GraphPad Prism. All figures were generated using Adobe Photoshop or Illustrator and model schematics were animated using BioRender.

## Supplementary Material

Refer to Web version on PubMed Central for supplementary material.

## ACKNOWLEDGMENTS

We thank the members of the Wells, Múnera, Zorn, and Daley laboratories for reagents and feedback. We acknowledge core support from the CCHMC Bioimaging and Analysis Facility (RRID:SCR_022628), Pluripotent Stem Cell Facility (RRID:SCR_022634), Single Cell Genomics Facility (RRID:SCR_022653), Transgenic Animal and Genome Editing Facility (RRID:SCR_022642), Genomics Sequencing Facility (RRID:SCR_022630), Integrated Pathology Research Facility (RRID:SCR_022637), and the Research Flow Cytometry Facility (RRID:SCR_022635). We thank Matt Kofron and the Bio-imaging and Analysis Facility (CCHMC) for training and guidance, Amy Pitstick from the Pluripotent Stem Cell Facility for cultures and reagents, and Kelly Rangel and Shawn Smith from the Single Cell Genomics Facility for scRNA-seq library preparation and advice. We would also like to thank the research cores at MUSC, including the Cell Models Core and the Advanced Imaging Core at MUSC. This research was supported by the grants from the NIH, U18 EB021780 (J.M.W. and M.A.H.), U19 AI116491 (J.M.W.), P01 HD093363 (J.M.W.), UG3 DK119982 (J.M.W.), U01 DK103117 (M.A.H.), NIEHS 5T32-ES007250–29 (D.O.K.), the Shipley Foundation (J.M.W.), and the Allen Foundation (J.M.W.). We also received support from the Digestive Disease Research Center (P30 DK078392). In addition, this research received support (J.O.M.) from the MUSC COBRE CDLD (P20 GM130457) and DDRCC (P30 DK123704).

## REFERENCES


1. Bain CC, Bravo-Blas A, Scott CL, Perdiguero EG, Geissmann F, Henri S, Malissen B, Osborne LC, Artis D, and Mowat AM (2014). Constant replenishment from circulating monocytes maintains the macrophage pool in the intestine of adult mice. Nat. Immunol 15, 929–937. 10.1038/ni.2967. [PubMed: 25151491]
2. Gomez Perdiguero E, Klapproth K, Schulz C, Busch K, Azzoni E, Crozet L, Garner H, Trouillet C, de Bruijn MF, Geissmann F, and Rodewald HR (2015). Tissue-resident macrophages originate from yolk-sac-derived erythro-myeloid progenitors. Nature 518, 547–551. 10.1038/nature13989. [PubMed: 25470051]
3. Hoeffel G, Chen J, Lavin Y, Low D, Almeida FF, See P, Beaudin AE, Lum J, Low I, Forsberg EC, et al. (2015). C-Myb(+) erythro-myeloid progenitor-derived fetal monocytes give rise to adult tissue-resident macrophages. Immunity 42, 665–678. 10.1016/j.im-muni.2015.03.011. [PubMed: 25902481]
4. Sheng J, Ruedl C, and Karjalainen K (2015). Most tissue-resident macrophages except microglia are derived from fetal hematopoietic stem cells. Immunity 43, 382–393. 10.1016/j.immuni.2015.07.016. [PubMed: 26287683]
5. Lazarov T, Juarez-Carreño S, Cox N, and Geissmann F (2023). Physiology and diseases of tissue-resident macrophages. Nature 618, 698–707. 10.1038/s41586-023-06002-x. [PubMed: 37344646]
6. Mass E, Ballesteros I, Farlik M, Halbritter F, Günther P, Crozet L, Jacome-Galarza CE, Händler K, Klughammer J, Kobayashi Y, et al. (2016). Specification of tissue-resident macrophages during organogenesis. Science 353, aaf4238. 10.1126/science.aaf4238. [PubMed: 27492475]
7. De Schepper S, Verheijden S, Aguilera-Lizarraga J, Viola MF, Boesmans W, Stakenborg N, Voytyuk I, Smidt I, Boeckx B, Dierckx de Casterlé I, et al. (2018). Self-maintaining gut macrophages are essential for intestinal homeostasis. Cell 175, 400–415.e13. 10.1016/j.cell.2018.07.048. [PubMed: 30173915]
8. Bujko A, Atlasy N, Landsverk OJB, Richter L, Yaqub S, Horneland R, Øyen O, Aandahl EM, Aabakken L, Stunnenberg HG, et al. (2018). Transcriptional and functional profiling defines human small intestinal macrophage subsets. J. Exp. Med 215, 441–458. [PubMed: 29273642]
9. Shaw TN, Houston SA, Wemyss K, Bridgeman HM, Barbera TA, Zangerle-Murray T, Strangward P, Ridley AJL, Wang P, Tamoutounour S, et al. (2018). Tissue-resident macrophages in the intestine are long lived and defined by Tim-4 and CD4 expression. J. Exp. Med 215, 1507–1518. [PubMed: 29789388]
10. Dick SA, Wong A, Hamidzada H, Nejat S, Nechanitzky R, Vohra S, Mueller B, Zaman R, Kantores C, Aronoff L, et al. (2022). Three tissue resident macrophage subsets coexist across organs with conserved origins and life cycles. Sci. Immunol 7, eabf7777. 10.1126/sciimmunol.abf7777. [PubMed: 34995099]
11. Dzierzak E, and Bigas A (2018). Blood development: hematopoietic stem cell dependence and independence. Cell Stem Cell 22, 639–651. 10.1016/j.stem.2018.04.015. [PubMed: 29727679]
12. Dzierzak E, and Speck NA (2008). Of lineage and legacy: the development of mammalian hematopoietic stem cells. Nat. Immunol 9, 129–136. 10.1038/ni1560. [PubMed: 18204427]
13. Perdiguero EG, and Geissmann F (2016). The development and maintenance of resident macrophages. Nat. Immunol 17, 2–8. 10.1038/ni.3341. [PubMed: 26681456]
14. Goh I, Botting RA, Rose A, Webb S, Engelbert J, Gitton Y, Stephenson E, Quiroga Londoño M, Mather M, Mende N, et al. (2023). Yolk sac cell atlas reveals multiorgan functions during human early development. Science 381, eadd7564. 10.1126/sci-ence.add7564. [PubMed: 37590359]
15. Bian Z, Gong Y, Huang T, Lee CZW, Bian L, Bai Z, Shi H, Zeng Y, Liu C, He J, et al. (2020). Deciphering human macrophage development at single-cell resolution. Nature 582, 571–576. 10.1038/s41586-020-2316-7. [PubMed: 32499656]
16. Calvanese V, Capellera-Garcia S, Ma F, Fares I, Liebscher S, Ng ES, Ekstrand S, Aguadé-Gorgorió J, Vavilina A, Lefaudeux D, et al. (2022). Mapping human haematopoietic stem cells from haemogenic endothelium to birth. Nature 604, 534–540. 10.1038/s41586-022-04571-x. [PubMed: 35418685]

17. Zeng Y, He J, Bai Z, Li Z, Gong Y, Liu C, Ni Y, Du J, Ma C, Bian L, et al. (2019). Tracing the first hematopoietic stem cell generation in human embryo by single-cell RNA sequencing. Cell Res 29, 881–894. 10.1038/s41422-019-0228-6. [PubMed: 31501518]

18. Cumano A, Dieterlen-Lievre F, and Godin I (1996). Lymphoid potential, probed before circulation in mouse, is restricted to caudal intraembryonic splanchnopleura. Cell 86, 907–916. [PubMed: 8808626]

19. Atkins MH, Scarfò R, McGrath KE, Yang D, Palis J, Ditadi A, and Keller GM (2022). Modeling human yolk sac hematopoiesis with pluripotent stem cells. J. Exp. Med 219, e20211924. 10.1084/jem.20211924. [PubMed: 34928315]

20. Jung HS, Uenishi G, Park MA, Liu P, Suknuntha K, Raymond M, Choi YJ, Thomson JA, Ong IM, and Slukvin II (2021). SOX17 integrates HOXA and arterial programs in hemogenic endothelium to drive definitive lympho-myeloid hematopoiesis. Cell Rep 34, 108758. 10.1016/j.celrep.2021.108758. [PubMed: 33596423]

21. Coşkun S, Chao H, Vasavada H, Heydari K, Gonzales N, Zhou X, de Crombrugghe B, and Hirschi KK (2014). Development of the fetal bone marrow niche and regulation of HSC quiescence and homing ability by emerging osteolineage cells. Cell Rep 9, 581–590. 10.1016/j.celrep.2014.09.013. [PubMed: 25310984]

22. Ciriza J, Thompson H, Petrosian R, Manilay JO, and García-Ojeda ME (2013). The migration of hematopoietic progenitors from the fetal liver to the fetal bone marrow: lessons learned and possible clinical applications. Exp. Hematol 41, 411–423. 10.1016/j.exphem.2013.01.009. [PubMed: 23395775]

23. Zanjani ED, Ascensao JL, and Tavassoli M (1993). Liver-derived fetal hematopoietic stem cells selectively and preferentially home to the fetal bone marrow. Blood 81, 399–404. [PubMed: 8093667]

24. Ara T, Tokoyoda K, Sugiyama T, Egawa T, Kawabata K, and Nagasawa T (2003). Long-term hematopoietic stem cells require stromal cell-derived factor-1 for colonizing bone marrow during ontogeny. Immunity 19, 257–267. 10.1016/s1074-7613(03)00201-2. [PubMed: 12932359]

25. Kennedy M, Awong G, Sturgeon CM, Ditadi A, LaMotte-Mohs R, Zúñiga-Pflücker JC, and Keller G (2012). T lymphocyte potential marks the emergence of definitive hematopoietic progenitors in human pluripotent stem cell differentiation cultures. Cell Rep 2, 1722–1735. 10.1016/j.celrep.2012.11.003. [PubMed: 23219550]

26. Sturgeon CM, Ditadi A, Awong G, Kennedy M, and Keller G (2014). Wnt signaling controls the specification of definitive and primitive hematopoiesis from human pluripotent stem cells. Nat. Biotechnol 32, 554–561. [PubMed: 24837661]

27. Choi KD, Vodyanik M, and Slukvin II (2011). Hematopoietic differentiation and production of mature myeloid cells from human pluripotent stem cells. Nat. Protoc 6, 296–313. 10.1038/nprot.2010.184. [PubMed: 21372811]

28. Lengerke C, Grauer M, Niebuhr NI, Riedt T, Kanz L, Park IH, and Daley GQ (2009). Hematopoietic development from human induced pluripotent stem cells. Ann. N. Y. Acad. Sci 1176, 219–227. 10.1111/j.1749-6632.2009.04606.x. [PubMed: 19796250]

29. Ng ES, Azzola L, Bruveris FF, Calvanese V, Phipson B, Vlahos K, Hirst C, Jokubaitis VJ, Yu QC, Maksimovic J, et al. (2016). Differentiation of human embryonic stem cells to HOXA(+) hemogenic vasculature that resembles the aorta-gonad-mesonephros. Nat. Biotechnol 34, 1168–1179. 10.1038/nbt.3702. [PubMed: 27748754]

30. Dou DR, Calvanese V, Sierra MI, Nguyen AT, Minasian A, Saarikoski P, Sasidharan R, Ramirez CM, Zack JA, Crooks GM, et al. (2016). Medial HOXA genes demarcate haematopoietic stem cell fate during human development. Nat. Cell Biol 18, 595–606. 10.1038/ncb3354. [PubMed: 27183470]

31. Sugimura R, Jha DK, Han A, Soria-Valles C, da Rocha EL, Lu YF, Goettel JA, Serrao E, Rowe RG, Malleshaiah M, et al. (2017). Haematopoietic stem and progenitor cells from human pluripotent stem cells. Nature 545, 432–438. 10.1038/nature22370. [PubMed: 28514439]

32. Tan YT, Ye L, Xie F, Beyer AI, Muench MO, Wang J, Chen Z, Liu H, Chen SJ, and Kan YW (2018). Respecifying human iPSC-derived blood cells into highly engraftable hematopoietic stem and progenitor cells with a single factor. Proc. Natl. Acad. Sci. USA 115, 2180–2185. 10.1073/pnas.1718446115. [PubMed: 29386396]

33. Kim J, Koo BK, and Knoblich JA (2020). Human organoids: model systems for human biology and medicine. Nat. Rev. Mol. Cell Biol 21, 571–584. 10.1038/s41580-020-0259-3. [PubMed: 32636524]
34. McCracken KW, Aihara E, Martin B, Crawford CM, Broda T, Treguier J, Zhang X, Shannon JM, Montrose MH, and Wells JM (2017). Wnt/beta-catenin promotes gastric fundus specification in mice and humans. Nature 541, 182–187. 10.1038/nature21021. [PubMed: 28052057]
35. McCracken KW, Catá EM, Crawford CM, Sinagoga KL, Schumacher M, Rockich BE, Tsai YH, Mayhew CN, Spence JR, Zavros Y, et al. (2014). Modelling human development and disease in pluripotent stem-cell-derived gastric organoids. Nature 516, 400–404. 10.1038/nature13863. [PubMed: 25363776]
36. Múnera JO, Sundaram N, Rankin SA, Hill D, Watson C, Mahe M, Vallance JE, Shroyer NF, Sinagoga KL, Zarzoso-Lacoste A, et al. (2017). Differentiation of human pluripotent stem cells into colonic organoids via transient activation of BMP signaling. Cell Stem Cell 21, 51–64.e6. 10.1016/j.stem.2017.05.020. [PubMed: 28648364]
37. Spence JR, Mayhew CN, Rankin SA, Kuhar MF, Vallance JE, Tolle K, Hoskins EE, Kalinichenko VV, Wells SI, Zorn AM, et al. (2011). Directed differentiation of human pluripotent stem cells into intestinal tissue in vitro. Nature 470, 105–109. 10.1038/nature09691. [PubMed: 21151107]
38. Trisno SL, Philo KED, McCracken KW, Catá EM, Ruiz-Torres S, Rankin SA, Han L, Nasr T, Chaturvedi P, Rothenberg ME, et al. (2018). Esophageal organoids from human pluripotent stem cells delineate Sox2 functions during esophageal specification. Cell Stem Cell 23, 501–515.e7. 10.1016/j.stem.2018.08.008. [PubMed: 30244869]
39. Lancaster MA, Renner M, Martin CA, Wenzel D, Bicknell LS, Hurles ME, Homfray T, Penninger JM, Jackson AP, and Knoblich JA (2013). Cerebral organoids model human brain development and microcephaly. Nature 501, 373–379. 10.1038/nature12517. [PubMed: 23995685]
40. Takasato M, Er PX, Chiu HS, Maier B, Baillie GJ, Ferguson C, Parton RG, Wolvetang EJ, Roost MS, Lopes SM, and Little MH (2016). Kidney organoids from human iPS cells contain multiple lineages and model human nephrogenesis. Nature 536, 238. 10.1038/nature17982.
41. Lewis-Israeli YR, Wasserman AH, Gabalski MA, Volmert BD, Ming Y, Ball KA, Yang W, Zou J, Ni G, Pajares N, et al. (2021). Self-assembling human heart organoids for the modeling of cardiac development and congenital heart disease. Nat. Commun 12, 5142. 10.1038/s41467-021-25329-5. [PubMed: 34446706]
42. Wills A, Dickinson K, Khokha M, and Baker JC (2008). Bmp signaling is necessary and sufficient for ventrolateral endoderm specification in Xenopus. Dev. Dyn 237, 2177–2186. 10.1002/dvdy.21631. [PubMed: 18651654]
43. Tiso N, Filippi A, Pauls S, Bortolussi M, and Argenton F (2002). BMP signalling regulates anteroposterior endoderm patterning in zebrafish. Mech. Dev 118, 29–37. [PubMed: 12351167]
44. Roberts DJ, Johnson RL, Burke AC, Nelson CE, Morgan BA, and Tabin C (1995). Sonic hedgehog is an endodermal signal inducing Bmp-4 and hox genes during induction and regionalization of the chick hindgut. Development 121, 3163–3174. [PubMed: 7588051]
45. Holloway EM, Wu JH, Czerwinski M, Sweet CW, Wu A, Tsai YH, Huang S, Stoddard AE, Capeling MM, Glass I, and Spence JR (2020). Differentiation of human intestinal organoids with endogenous vascular endothelial cells. Dev. Cell 54, 516–528.e7. 10.1016/j.devcel.2020.07.023. [PubMed: 32841595]
46. Minegishi N, Ohta J, Yamagiwa H, Suzuki N, Kawauchi S, Zhou Y, Takahashi S, Hayashi N, Engel JD, and Yamamoto M (1999). The mouse GATA-2 gene is expressed in the para-aortic splanchnopleura and aorta-gonads and mesonephros region. Blood 93, 4196–4207. [PubMed: 10361117]
47. Wang Q, Stacy T, Binder M, Marin-Padilla M, Sharpe AH, and Speck NA (1996). Disruption of the Cbfa2 gene causes necrosis and hemorrhaging in the central nervous system and blocks definitive hematopoiesis. Proc. Natl. Acad. Sci. USA 93, 3444–3449. [PubMed: 8622955]
48. North TE, de Bruijn MF, Stacy T, Talebian L, Lind E, Robin C, Binder M, Dzierzak E, and Speck NA (2002). Runx1 expression marks long-term repopulating hematopoietic stem cells in the midgestation mouse embryo. Immunity 16, 661–672. 10.1016/s1074-7613(02)00296-0. [PubMed: 12049718]

49. Crosse EI, Gordon-Keylock S, Rybtsov S, Binagui-Casas A, Felchle H, Nnadi NC, Kirschner K, Chandra T, Tamagno S, Webb DJ, et al. (2020). Multi-layered spatial transcriptomics identify secretory factors promoting human hematopoietic stem cell development. Cell Stem Cell 27, 822–839.e8. 10.1016/j.stem.2020.08.004. [PubMed: 32946788]
50. Choi KD, Vodyanik MA, Togarrati PP, Suknuntha K, Kumar A, Samarjeet F, Probasco MD, Tian S, Stewart R, Thomson JA, and Slukvin II (2012). Identification of the hemogenic endothelial progenitor and its direct precursor in human pluripotent stem cell differentiation cultures. Cell Rep 2, 553–567. 10.1016/j.celrep.2012.08.002. [PubMed: 22981233]
51. Popescu DM, Botting RA, Stephenson E, Green K, Webb S, Jardine L, Calderbank EF, Polanski K, Goh I, Efremova M, et al. (2019). Decoding human fetal liver haematopoiesis. Nature 574, 365–371. 10.1038/s41586-019-1652-y. [PubMed: 31597962]
52. Peeters M, Ottersbach K, Bollerot K, Orelio C, de Bruijn M, Wijgerde M, and Dzierzak E (2009). Ventral embryonic tissues and Hedgehog proteins induce early AGM hematopoietic stem cell development. Development 136, 2613–2621. 10.1242/dev.034728. [PubMed: 19570846]
53. Gao N, White P, and Kaestner KH (2009). Establishment of intestinal identity and epithelial-mesenchymal signaling by Cdx2. Dev. Cell 16, 588–599. 10.1016/j.devcel.2009.02.010. [PubMed: 19386267]
54. Grainger S, Savory JG, and Lohnes D (2010). Cdx2 regulates patterning of the intestinal epithelium. Dev. Biol 339, 155–165. 10.1016/j.ydbio.2009.12.025. [PubMed: 20043902]
55. Kumar N, Tsai YH, Chen L, Zhou A, Banerjee KK, Saxena M, Huang S, Toke NH, Xing J, Shivdasani RA, et al. (2019). The lineage-specific transcription factor CDX2 navigates dynamic chromatin to control distinct stages of intestine development. Development 146, dev172189. 10.1242/dev.172189. [PubMed: 30745430]
56. Mendjan S, Mascetti VL, Ortmann D, Ortiz M, Karjosukarso DW, Ng Y, Moreau T, and Pedersen RA (2014). NANOG and CDX2 pattern distinct subtypes of human mesoderm during exit from pluripotency. Cell Stem Cell 15, 310–325. 10.1016/j.stem.2014.06.006. [PubMed: 25042702]
57. Yu Q, Kilik U, Holloway EM, Tsai YH, Harmel C, Wu A, Wu JH, Czerwinski M, Childs CJ, He Z, et al. (2021). Charting human development using a multi-endodermal organ atlas and organoid models. Cell 184, 3281–3298.e22. 10.1016/j.cell.2021.04.028. [PubMed: 34019796]
58. Wang Y, Yabuuchi A, McKinney-Freeman S, Ducharme DM, Ray MK, Chawengsaksophak K, Archer TK, and Daley GQ (2008). Cdx gene deficiency compromises embryonic hematopoiesis in the mouse. Proc. Natl. Acad. Sci. USA 105, 7756–7761. 10.1073/pnas.0708951105. [PubMed: 18511567]
59. Ginhoux F, and Guilliams M (2016). Tissue-resident macrophage ontogeny and homeostasis. Immunity 44, 439–449. 10.1016/j.immuni.2016.02.024. [PubMed: 26982352]
60. Uhlén M, Björling E, Agaton C, Szigyarto CA-K, Amini B, Andersen E, Andersson A-C, Angelidou P, Asplund A, Asplund C, et al. (2005). A human protein atlas for normal and cancer tissues based on antibody proteomics. Mol. Cell. Proteomics 4, 1920–1932. [PubMed: 16127175]
61. Bulmer JN, and Johnson PM (1984). Macrophage populations in the human placenta and amniochorion. Clin. Exp. Immunol 57, 393–403. [PubMed: 6380834]
62. Davies LC, Jenkins SJ, Allen JE, and Taylor PR (2013). Tissue-resident macrophages. Nat. Immunol 14, 986–995. 10.1038/ni.2705. [PubMed: 24048120]
63. Kotlarz D, Beier R, Murugan D, Diestelhorst J, Jensen O, Boztug K, Pfeifer D, Kreipe H, Pfister ED, Baumann U, et al. (2012). Loss of interleukin-10 signaling and infantile inflammatory bowel disease: implications for diagnosis and therapy. Gastroenterology 143, 347–355. 10.1053/j.gastro.2012.04.045. [PubMed: 22549091]
64. Kühn R, Löhler J, Rennick D, Rajewsky K, and Müller W (1993). Interleukin-10-deficient mice develop chronic enterocolitis. Cell 75, 263–274. 10.1016/0092-8674(93)80068-p. [PubMed: 8402911]
65. Moran CJ, Walters TD, Guo CH, Kugathasan S, Klein C, Turner D, Wolters VM, Bandsma RH, Mouzaki M, Zachos M, et al. (2013). IL-10R polymorphisms are associated with very-early-onset ulcerative colitis. Inflam. Bowel Dis 19, 115–123. 10.1002/ibd.22974.
66. Zigmond E, Bernshtein B, Friedlander G, Walker CR, Yona S, Kim K-W, Brenner O, Krauthgamer R, Varol C, Müller W, and Jung S (2014). Macrophage-restricted interleukin-10 receptor

deficiency, but not IL-10 deficiency, causes severe spontaneous colitis. Immunity 40, 720–733. [PubMed: 24792913]

67. Shouval DS, Biswas A, Goettel JA, McCann K, Conaway E, Redhu NS, Mascanfroni ID, Al Adham Z, Lavoie S, Ibourk M, et al. (2014). Interleukin-10 receptor signaling in innate immune cells regulates mucosal immune tolerance and anti-inflammatory macrophage function. Immunity 40, 706–719. [PubMed: 24792912]
68. Krause P, Morris V, Greenbaum JA, Park Y, Bjoerheden U, Mikulski Z, Muffley T, Shui JW, Kim G, Cheroutre H, et al. (2015). IL-10-producing intestinal macrophages prevent excessive anti-bacterial innate immunity by limiting IL-23 synthesis. Nat. Commun 6, 7055. 10.1038/ncomms8055. [PubMed: 25959063]
69. Biswas A, Shouval DS, Griffith A, Goettel JA, Field M, Kang YH, Konnikova L, Janssen E, Redhu NS, Thrasher AJ, et al. (2018). WASP-mediated regulation of anti-inflammatory macrophages is IL-10 dependent and is critical for intestinal homeostasis. Nat. Commun 9, 1779. 10.1038/s41467-018-03670-6. [PubMed: 29725003]
70. Qu N, Jeffcoat B, Maity P, Christensen RK, and Múnera JO (2022). Retinoic acid promotes the in vitro growth, patterning and improves the cellular composition of human pluripotent stem-cell-derived intestinal organoids. Int. J. Mol. Sci 23, 8624. 10.3390/ijms23158624. [PubMed: 35955755]
71. Maheshwari A, Kelly DR, Nicola T, Ambalavanan N, Jain SK, Murphy-Ullrich J, Athar M, Shimamura M, Bhandari V, Aprahamian C, et al. (2011). TGF-beta2 suppresses macrophage cytokine production and mucosal inflammatory responses in the developing intestine. Gastroenterology 140, 242–253. [PubMed: 20875417]
72. Wright SD, Ramos RA, Tobias PS, Ulevitch RJ, and Mathison JC (1990). CD14, a receptor for complexes of lipopolysaccharide (LPS) and LPS binding protein. Science 249, 1431–1433. 10.1126/science.1698311. [PubMed: 1698311]
73. Haziot A, Ferrero E, Köntgen F, Hijiya N, Yamamoto S, Silver J, Stewart CL, and Goyert SM (1996). Resistance to endotoxin shock and reduced dissemination of gram-negative bacteria in CD14-deficient mice. Immunity 4, 407–414. 10.1016/s1074-7613(00)80254-x. [PubMed: 8612135]
74. Bain CC, and Schridde A (2018). Origin, differentiation, and function of intestinal macrophages. Front. Immunol 9, 2733. 10.3389/fimmu.2018.02733. [PubMed: 30538701]
75. Flannagan RS, Jaumouillé V, and Grinstein S (2012). The cell biology of phagocytosis. Annu. Rev. Pathol 7, 61–98. 10.1146/annurev-pathol-011811-132445. [PubMed: 21910624]
76. Man AL, Gicheva N, Regoli M, Rowley G, De Cunto G, Wellner N, Bassity E, Gulisano M, Bertelli E, and Nicoletti C (2017). CX3CR1+ cell-mediated salmonella exclusion protects the intestinal mucosa during the initial stage of infection. J. Immunol 198, 335–343. 10.4049/jimmunol.1502559. [PubMed: 27895168]
77. Singh A, Poling HM, Sundaram N, Brown N, Wells JM, and Helmrath MA (2020). Evaluation of transplantation sites for human intestinal organoids. PLoS One 15, e0237885. 10.1371/journal.pone.0237885. [PubMed: 32853234]
78. Watson CL, Mahe MM, Múnera J, Howell JC, Sundaram N, Poling HM, Schweitzer JI, Vallance JE, Mayhew CN, Sun Y, et al. (2014). An in vivo model of human small intestine using pluripotent stem cells. Nat. Med 20, 1310–1314. 10.1038/nm.3737. [PubMed: 25326803]
79. Maeno M, Mead PE, Kelley C, Xu RH, Kung HF, Suzuki A, Ueno N, and Zon LI (1996). The role of BMP-4 and GATA-2 in the induction and differentiation of hematopoietic mesoderm in Xenopus laevis. Blood 88, 1965–1972. [PubMed: 8822915]
80. Ormel PR, Vieira de Sá R, van Bodegraven EJ, Karst H, Harschnitz O, Sneeboer MAM, Johansen LE, van Dijk RE, Scheefhals N, Berdenis van Berlekom A, et al. (2018). Microglia innately develop within cerebral organoids. Nature communications 9, 4167. 10.1038/s41467-018-06684-2.
81. Michaelson MD, Bieri PL, Mehler MF, Xu H, Arezzo JC, Pollard JW, and Kessler JA (1996). CSF-1 deficiency in mice results in abnormal brain development. Development 122, 2661–2672. [PubMed: 8787741]
82. Pollard JW (2009). Trophic macrophages in development and disease. Nat. Rev. Immunol 9, 259–270. 10.1038/nri2528. [PubMed: 19282852]

83. Gouon-Evans V, Rothenberg ME, and Pollard JW (2000). Postnatal mammary gland development requires macrophages and eosinophils. Development 127, 2269–2282. [PubMed: 10804170]
84. Dai XM, Ryan GR, Hapel AJ, Dominguez MG, Russell RG, Kapp S, Sylvestre V, and Stanley ER (2002). Targeted disruption of the mouse colony-stimulating factor 1 receptor gene results in osteopetrosis, mononuclear phagocyte deficiency, increased primitive progenitor cell frequencies, and reproductive defects. Blood 99, 111–120. 10.1182/blood.v99.1.111. [PubMed: 11756160]
85. Huynh D, Akçora D, Malaterre J, Chan CK, Dai XM, Bertoncello I, Stanley ER, and Ramsay RG (2013). CSF-1 receptor-dependent colon development, homeostasis and inflammatory stress response. PLoS One 8, e56951. 10.1371/journal.pone.0056951. [PubMed: 23451116]
86. Glocker E-O, Kotlarz D, Boztug K, Gertz EM, Schäffer AA, Noyan F, Perro M, Diestelhorst J, Allroth A, Murugan D, et al. (2009). Inflammatory bowel disease and mutations affecting the interleukin-10 receptor. N. Engl. J. Med 361, 2033–2045. [PubMed: 19890111]
87. Tugizov SM, Herrera R, Veluppillai P, Greenspan D, Soros V, Greene WC, Levy JA, and Palefsky JM (2012). Differential transmission of HIV traversing fetal oral/intestinal epithelia and adult oral epithelia. J. Virol 86, 2556–2570. 10.1128/JVI.06578-11. [PubMed: 22205732]
88. Campbell EL, Bruyninckx WJ, Kelly CJ, Glover LE, McNamee EN, Bowers BE, Bayless AJ, Scully M, Saeedi BJ, Golden-Mason L, et al. (2014). Transmigrating neutrophils shape the mucosal microenvironment through localized oxygen depletion to influence resolution of inflammation. Immunity 40, 66–77. 10.1016/j.im-muni.2013.11.020. [PubMed: 24412613]
89. Drokhlyansky E, Smillie CS, Van Wittenberghe N, Ericsson M, Griffin GK, Eraslan G, Dionne D, Cuoco MS, Goder-Reiser MN, Sharova T, et al. (2020). The human and mouse enteric nervous system at single-cell resolution. Cell 182, 1606–1622.e23. 10.1016/j.cell.2020.08.003. [PubMed: 32888429]
90. Holokai L, Chakrabarti J, Broda T, Chang J, Hawkins JA, Sundaram N, Wroblewski LE, Peek RM Jr., Wang J, Helmrath M, et al. (2019). Increased programmed death-ligand 1 is an early epithelial cell response to Helicobacter pylori infection. PLoS Pathog 15, e1007468. 10.1371/journal.ppat.1007468. [PubMed: 30703170]
91. Langmead B, Trapnell C, Pop M, and Salzberg SL (2009). Ultrafast and memory-efficient alignment of short DNA sequences to the human genome. Genome Biol 10, R25. 10.1186/gb-2009-10-3-r25. [PubMed: 19261174]
92. Trapnell C, Roberts A, Goff L, Pertea G, Kim D, Kelley DR, Pimentel H, Salzberg SL, Rinn JL, and Pachter L (2012). Differential gene and transcript expression analysis of RNA-seq experiments with TopHat and Cufflinks. Nat. Protoc 7, 562–578. 10.1038/nprot.2012.016. [PubMed: 22383036]
93. Butler A, Hoffman P, Smibert P, Papalexi E, and Satija R (2018). Integrating single-cell transcriptomic data across different conditions, technologies, and species. Nat. Biotechnol 36, 411–420. 10.1038/nbt.4096. [PubMed: 29608179]
94. Cao J, Spielmann M, Qiu X, Huang X, Ibrahim DM, Hill AJ, Zhang F, Mundlos S, Christiansen L, Steemers FJ, et al. (2019). The single-cell transcriptional landscape of mammalian organogenesis. Nature 566, 496–502. 10.1038/s41586-019-0969-x. [PubMed: 30787437]
95. Jin S, Guerrero-Juarez CF, Zhang L, Chang I, Ramos R, Kuan CH, Myung P, Plikus MV, and Nie Q (2021). Inference and analysis of cell-cell communication using CellChat. Nature communications 12, 1088. 10.1038/s41467-021-21246-9.
96. Thorner K, Zorn AM, and Chaturvedi P (2021). ELeFHAnt: A supervised machine learning approach for label harmonization and annotation of single cell RNA-seq data. bioRxiv. 2021.09.07.459342 10.1101/2021.09.07.459342.
97. Chen B, Gilbert LA, Cimini BA, Schnitzbauer J, Zhang W, Li GW, Park J, Blackburn EH, Weissman JS, Qi LS, and Huang B (2013). Dynamic imaging of genomic loci in living human cells by an optimized CRISPR/Cas system. Cell 155, 1479–1491. 10.1016/j.cell.2013.12.001. [PubMed: 24360272]
98. Slaymaker IM, Gao L, Zetsche B, Scott DA, Yan WX, and Zhang F (2016). Rationally engineered Cas9 nucleases with improved specificity. Science 351, 84–88. 10.1126/science.aad5227. [PubMed: 26628643]

99. McCauley HA, Matthis AL, Enriquez JR, Nichol JT, Sanchez JG, Stone WJ, Sundaram N, Helmrath MA, Montrose MH, Aihara E, and Wells JM (2020). Enteroendocrine cells couple nutrient sensing to nutrient absorption by regulating ion transport. Nat. Commun 11, 4791. 10.1038/s41467-020-18536-z. [PubMed: 32963229]

100. Becht E, McInnes L, Healy J, Dutertre CA, Kwok IWH, Ng LG, Ginhoux F, and Newell EW (2018). Dimensionality reduction for visualizing single-cell data using UMAP. Nat. Biotechnol 10.1038/nbt.4314.

101. Stuart T, Butler A, Hoffman P, Hafemeister C, Papalexi E, Mauck WM 3rd, Hao Y, Stoeckius M, Smibert P, and Satija R (2019). Comprehensive integration of single-cell data. Cell 177, 1888–1902.e21. 10.1016/j.cell.2019.05.031. [PubMed: 31178118]

102. Ditadi A, Sturgeon CM, Tober J, Awong G, Kennedy M, Yzaguirre AD, Azzola L, Ng ES, Stanley EG, French DL, et al. (2015). Human definitive haemogenic endothelium and arterial vascular endothelium represent distinct lineages. Nat. Cell Biol 17, 580–591. 10.1038/ncb3161. [PubMed: 25915127]

103. Bouffi C, Wikenheiser-Brokamp KA, Chaturvedi P, Sundaram N, Goddard GR, Wunderlich M, Brown NE, Staab JF, Latanich R, Zachos NC, et al. (2023). In vivo development of immune tissue in human intestinal organoids transplanted into humanized mice. Nat. Biotechnol 41, 824–831. 10.1038/s41587-022-01558-x. [PubMed: 36702898]

## Highlights

- BMP induces HE-like cells in hPSC-derived HCOs
- HE begets erythromyeloid progenitors that can differentiate into macrophages
- Macrophages respond to pro-inflammatory signals and secrete cytokines
- Macrophages in HCOs transcriptionally resemble those found in human fetal colon

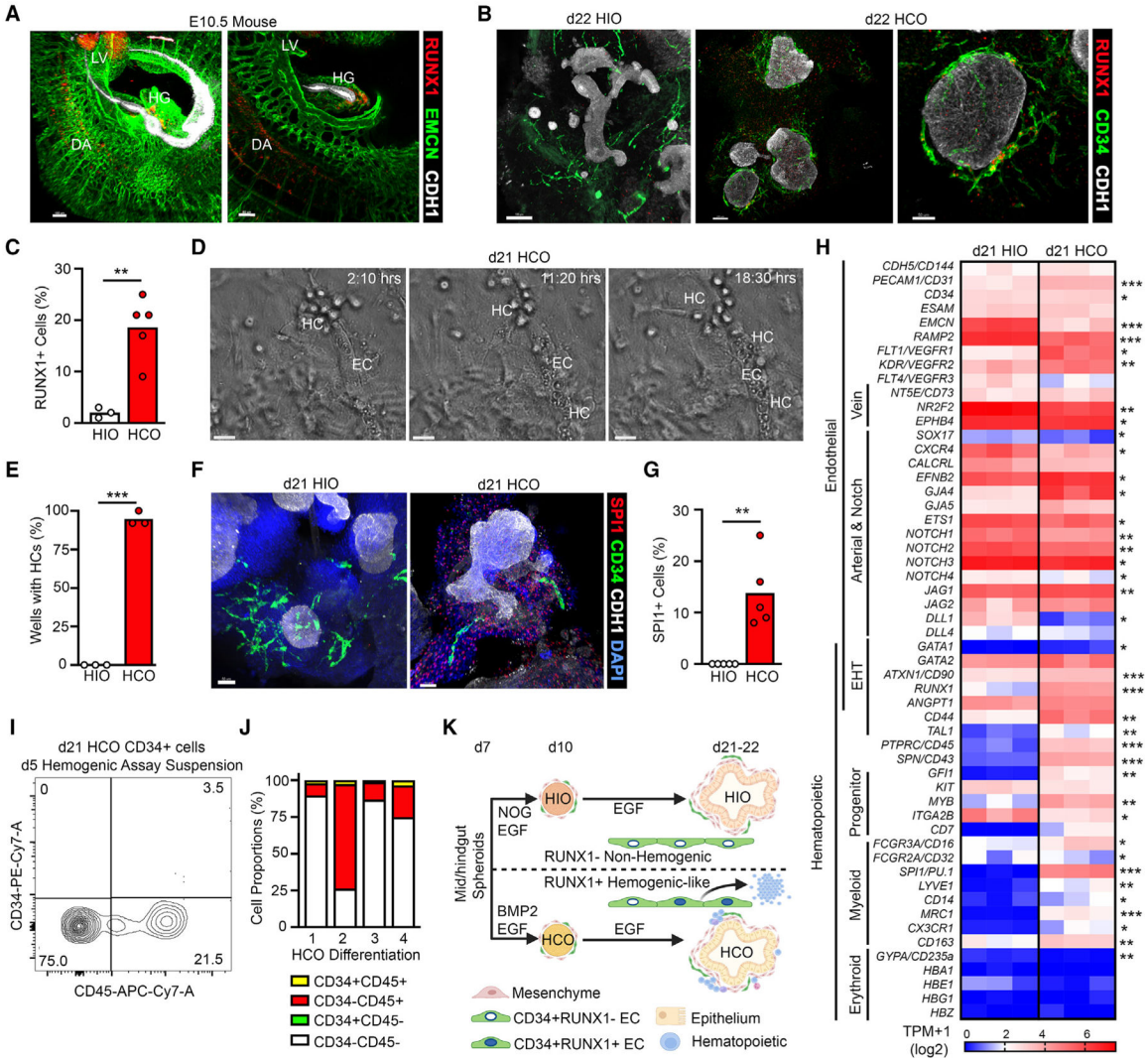


**Figure 1. HE-like cells co-developed in HCO cultures**

(A) Wholemount RUNX1 (red), ENDOMUCIN (green), and CDX2 (white) staining of an E10.5 mouse embryo. On the right, optical slices from wholemount showed nuclear RUNX1 staining in the dorsal aorta (DA) and around the hindgut (HG) and liver (Lv) endoderm (n = 3).

(B and C) (B) Wholemount RUNX1 (red), CD34 (green), and CDH1 (white) staining and (C) quantification of a day 22 HIO and HCOs showing nuclear RUNX1 staining within CD34+ endothelial tubes in HCOs (n = 3–5).

(D) Stereoscopic time-lapse snapshots from day 21 HCO mesenchyme showing an endothelial tube (EC) and hematopoietic cells (HCs) within EC's lumen (see Video S1).

(E) Stereoscopic quantification of the percentage of wells of a 24-well plate containing HIOs or HCOs containing HCs (n = 3 differentiations).

(F and G) (F) Immunofluorescent staining and (G) quantification of day 21 HIOs and HCOs for CD34 (green), SPI1 (red), and CDH1 (white) and counterstained with DAPI. A minimum of 5 organoids from each of 2 separate differentiations was analyzed.

(H) Relative expression in transcripts per million (TPM) of endothelial and hematopoietic genes from bulk RNA-seq data of day 21 HIOs and HCOs (n = 3 biological replicates, i.e., 3 separate differentiations).

(I) Representative flow cytometric analysis of cell suspension stained with CD45 and CD34 following 5 days of culture of isolated day 21 HCO CD34+ cells.

(J) Quantification of hemogenic assay across 4 separate differentiations.

(K) Schematic showing differences in HIO and HCO protocols. Significance determined by unpaired t test with *$p < 0.05$, **$p < 0.01$, ***$p < 0.001$ ($n = 3–5$). Scale bars: (A and B) 100 μm in wholemount; (A) 80 μm and (B and F) 50 μm in the optical slices; (D) 20 μm.

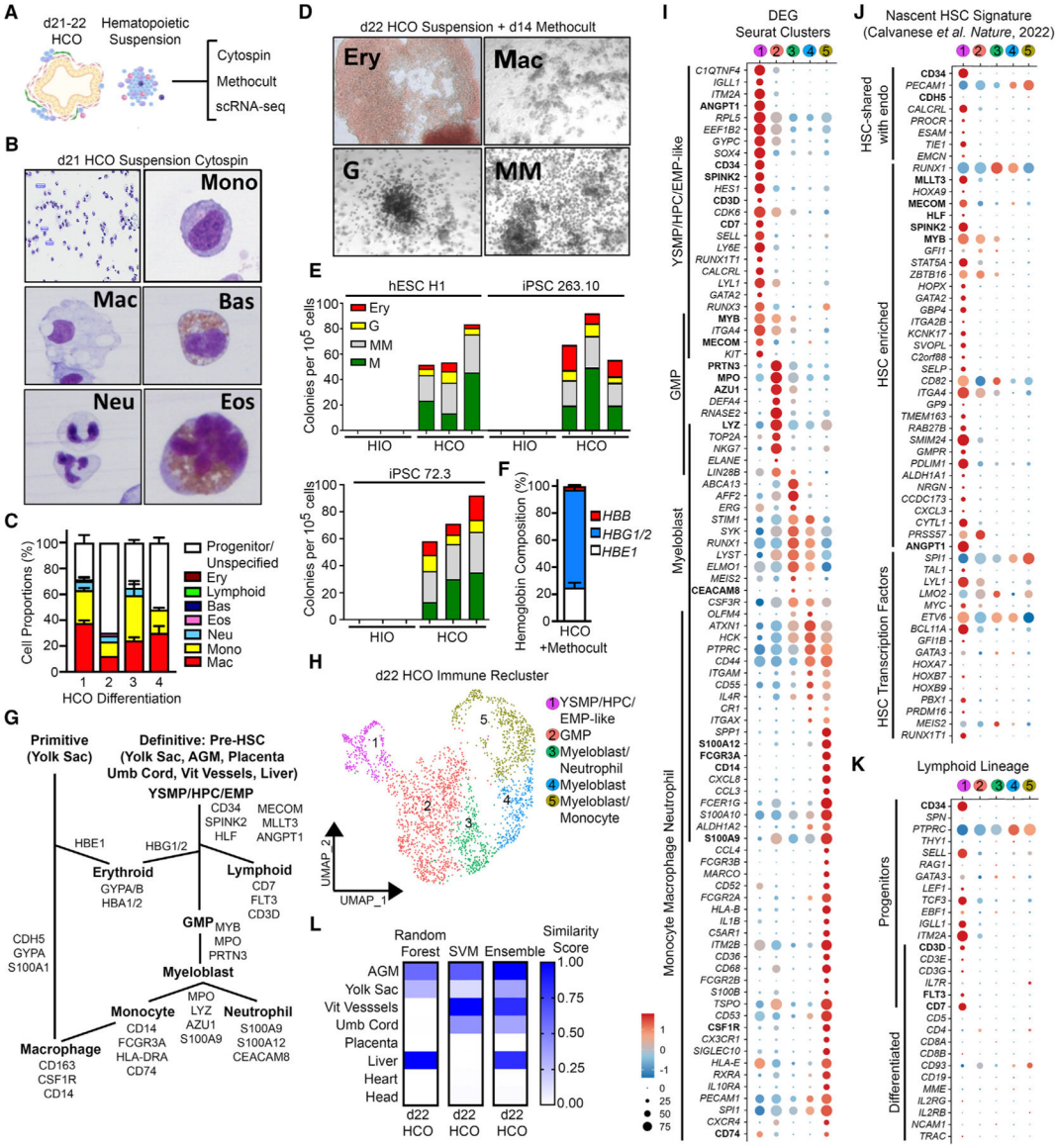


**Figure 2. HCO cultures contained pre-HSC EMPs**

(A) Schematic of assays performed on day 21 and 22 HCOs.

(B and C) (B) Micrographs of low and higher power magnification of cytospun cells from day 21 HCO cultures. Representative images and (C) quantification of monocytes (Mono), macrophages (Mac), neutrophils (Neu), basophils (Bas), and eosinophils (Eos), unspecified progenitors, erythrocytes (Ery), or lymphoid cells. Pictures and quantification are representative of 4 separate differentiations.

(D) Micrographs of colonies formed after day 21 and 22 HCO cell suspensions were cultured in Methocult medium. Representative images of Ery, Mac, granulocyte (G), and mixed myeloid (MM) colonies.

(E) Quantification of colony formation in Methocult from HIO and HCOs derived from H1 hESC and control iPSC lines. Results are from 3 biological replicates (colony forming assays from 3 separate differentiations).

(F) Relative hemoglobin expression (based on RT-qPCR) of embryonic/primitive HBE1, fetal HBG1/2, and adult HBB subunits from day 22 HCO suspended cells cultured in Methocult.

(G) Schematic of differentiation and associated markers of primitive and pre-HSC definitive waves of fetal hematopoiesis. Yolk sac multipotent progenitors (YSMPs), hematopoietic progenitor cells (HPCs), granulocyte-monocyte progenitor (GMP), vitelline vessels (Vit), and umbilical (Umb).

(H) Uniform manifold approximation and projection (UMAP) clustering of all hematopoietic cells from the day 22 HCO cultures.

(I–K) Relative expression and abundance of select (I) differential expressed genes (DEGs), (J) published nascent HSC signature,[16] and (K) lymphoid lineage markers in each Seurat cluster from day 22 HCO hematopoietic cells. Bolded genes are marker genes from (G).

(L) Deduced relationship between RNA expression of day 22 HCO hematopoietic cells and a published CS14 human fetal hematopoietic reference dataset.[16] Similarity score determined by both random forest (RF) and support vector machine (SVM) or a combination of both (ensemble).

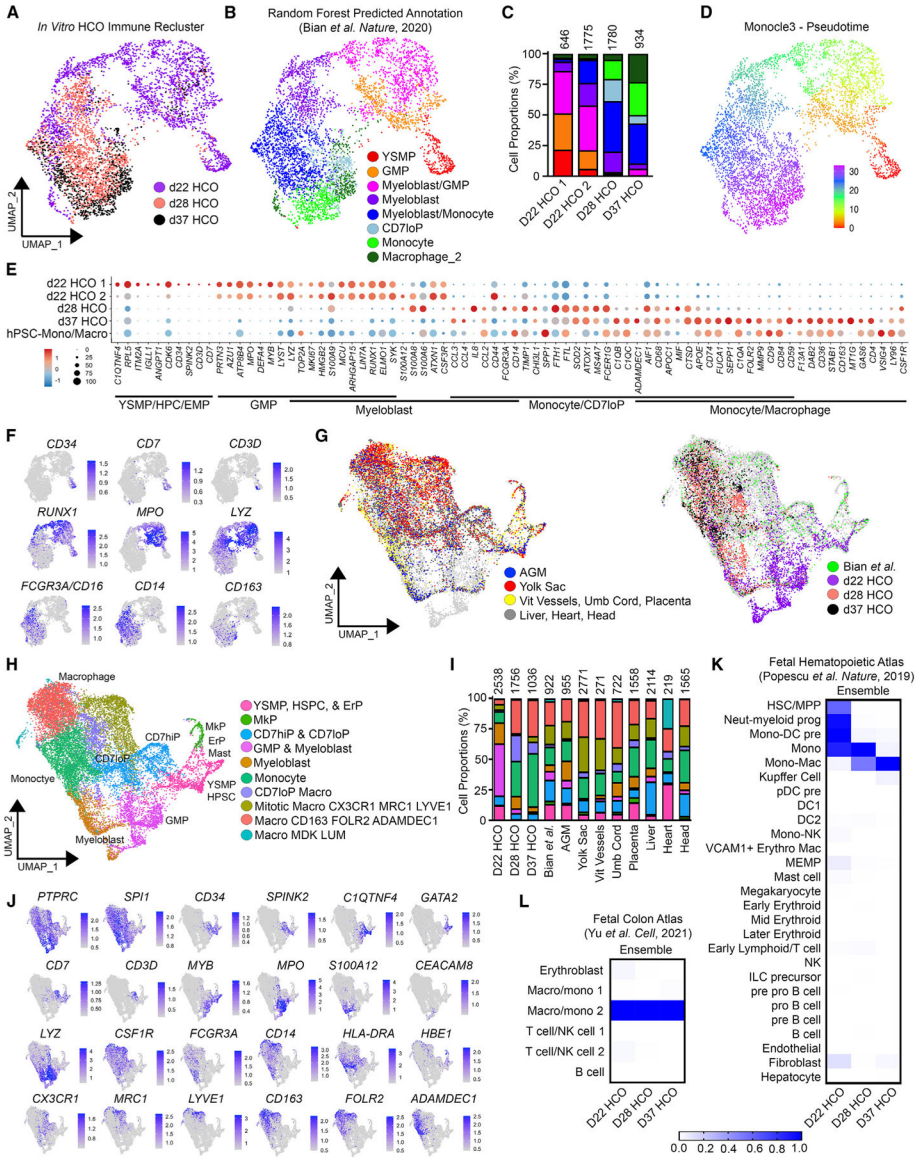


**Figure 3. The differentiation trajectory of macrophages in HCOs resembled that of human embryos**

(A and B) UMAP clustering of all hematopoietic cells integrated from the HCO cultures colored by (A) time point or (B) cell type based on random forest predictions using annotations from published fetal macrophage atlas.[15]

(C) Relative proportions of predicted cell types in each HCO sample. Numbers above bars represent the total number of hematopoietic cells in each condition.

(D) Pseudotime trajectory of day 22, day 28, and day 37 HCO hematopoietic cells.

(E and F) Dot or feature plots of relative expression and abundance of differentiation progression from HPCs and lymphoid cells (*CD34*, *CD7*, and *CD3D*) to GMP/myeloblast (*RUNX1*, *MPO*, and *LYZ*) to monocyte/macrophage (*FCGR3A*, *CD14*, and *CD163*). Monocytes/macrophages (hPSC-mono/macro) were derived independent of HCOs.

(G and H) UMAP clustering of all hematopoietic cells integrated from all three *in vitro* HCO time points and published fetal hematopoietic datasets[15,16] colored by (G) anatomical

sample (left: AGM, yolk sac, pooled vitelline vessels, umbilical cord, placenta or liver, heart, and lung; right; Bian et al. atlas, day 22, day 28, or day 37 HCOs) or (H) Seurat cluster annotated with cell types. Cell-type annotations from Bian et al. reference atlas include YSMP, hematopoietic stem/progenitor cells (HSPCs), erythroid (ErP), and megakaryocyte (MkP) progenitors; mast cells; lympho-myeloid CD7-high (CD7hiP) and -low (CD7loP) progenitors; GMP; myeloblasts; monocytes; and macrophage populations. Markers enriched in specific macrophage cluster are listed.

(I) Relative proportions of predicted cell types in each HCO sample and the macrophage[15] and CS14/4.5 week hematopoietic cell atlases.[16]

(J) Feature plots of select hematopoietic genes showing the distribution of in pan-immune (*PTPRC* and *SPI1*), HPCs (*CD34*, *SPINK2*, and *C1QTNF4*), ErP/MkP (*GATA2* and *HBE1*), CD7hiP/lymphoid (*CD7* and *CD3D*), GMP (*MYB* and *MPO*), myeloblast (*CEACAM8*, *LYZ*, and *S100A12*), monocyte (*CSF1R*, *FCGR3A*, *CD14*, and *HLA-DRA*), and macrophage (*CX3CR1*, *MRC1*, *LYVE1*, *CD163*, *FOLR2*, and *ADAMDEC1*).

(K and L) Ensemble similarity score of HCOs hematopoietic cells compared with annotations from (K) fetal hematopoietic[51] or (L) hematopoietic cells from fetal colon reference atlases.[57]

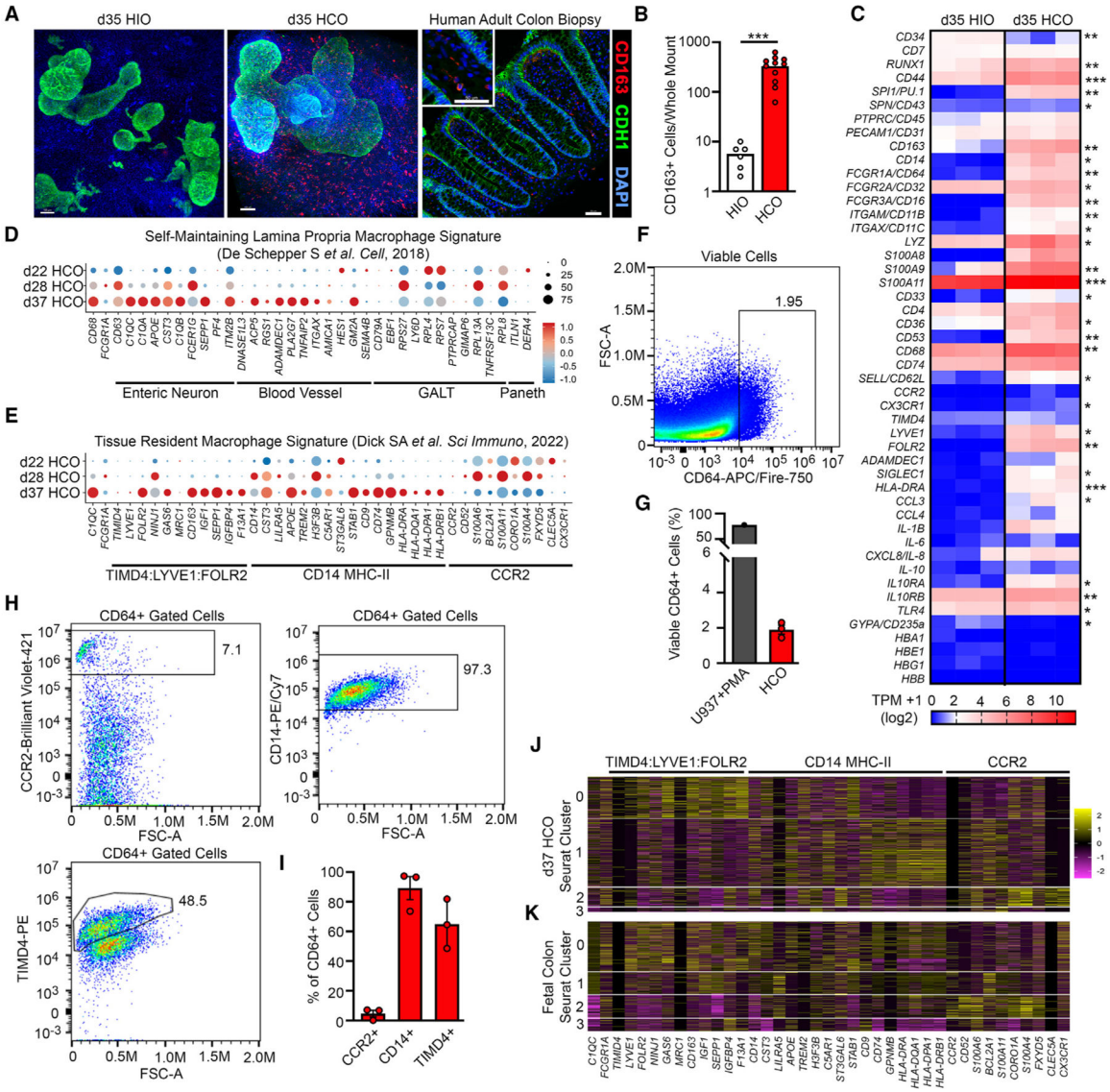


**Figure 4. HCO macrophages adopted a tissue-resident signature**

(A) Wholemount immunofluorescence of day 35 HIOs and HCOs or human colon biopsy stained for macrophage marker CD163 (red), epithelial CDH1 (green), and counterstained with DAPI (n = 2–11). Inset high magnification of human colonic biopsy macrophages.

(B) Quantification of CD163+ macrophage in day 35 HIO and HCO wholemounts (n = 6–11).

(C–E) (C) Relative expression in TPM of myeloid genes from bulk RNA-seq of day 35 HIOs and HCOs (n = 3 biological replicates). Relative expression of published

(D) self-maintaining lamina propria macrophages[7]or (E) tissue-resident macrophages[10] from day 22, day 28, and day 37 HCO immune cells from scRNA-seq.

(F and G) (F) Representative flow cytometric analysis and (G) quantification of gated viable cells expressing monocyte/macrophage marker FCGR1A/CD64 in day 35 HCOs (n = 3). U937 + PMA cells were used a positive control.

(H and I) (H) Flow cytometric analysis and (I) quantification of the percentage of gated viable CD64+ cells that co-express the macrophage markers CCR2/CD192, CD14, or TIMD4 from day 35 HCOs (n = 3).

(J and K) (J) Heatmap expression of tissue resident macrophage markers expressed in HCOs identified from atlas highlighted in (E) and (K) published fetal colon macrophages[57]. Significance *p < 0.05, **p < 0.01, ***p < 0.001 determined by t test. Scale bars: wholemount 100 μm and biopsy section 50 μm.

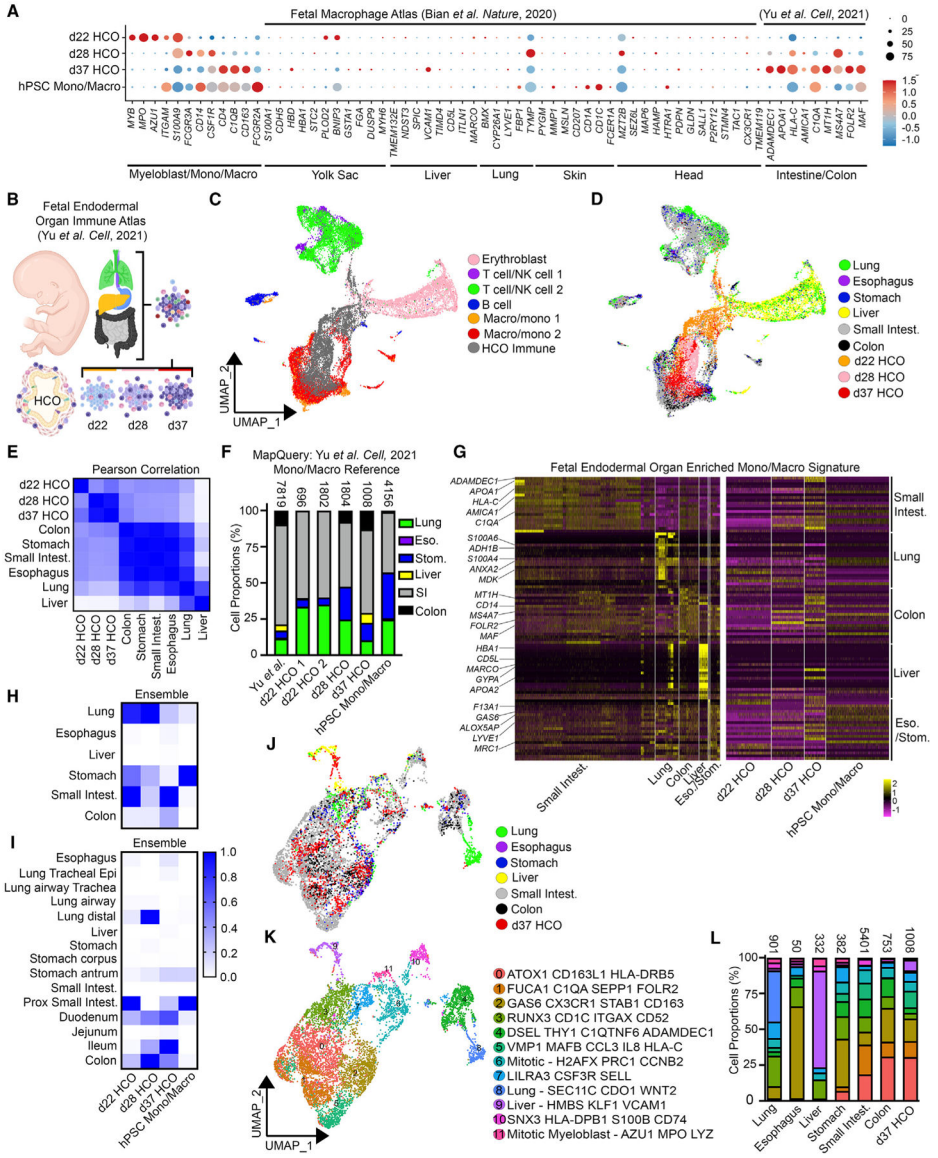


**Figure 5. Monocytes and macrophages in HCOs acquired an intestinal/colonic-like transcriptional signature**

(A) Relative expression and abundance of tissue-enriched macrophage markers from the yolk sac, liver, lung, skin, head, or intestine/colonic in day 22, day 28, and day 37 HCO hematopoietic cells or hPSC monocyte/macrophage (mono/macro). Enriched macrophage markers are identified by Bian et al. macrophage atlas or the Yu et al. endodermal atlas for the intestine/colon.

(B) Schematic of comparing HCOs to published hematopoietic cells from human fetal endodermal tissue atlas.[57]

(C and D) UMAP clustering of all hematopoietic cells integrated from all time points of *in vitro* HCO cultures and human fetal tissues. UMAPs colored by (C) annotated cell types or (D) organ.

(E) Pearson correlation of all RNA from all hematopoietic cells in HCOs and fetal endodermal organs.

(F) Relative proportions of HCO hematopoietic cells or hPSC mono/macro that mapped onto reference fetal mono/macro annotated cells from each organ.[57] Mono/macro and organ annotations from reference atlas.

(G) Heatmap of the top 20 differentially expressed genes of individual organs from all mono/macro annotated cells from human fetal endodermal atlas across all time points. Same genes in day 22, day 28, and day 37 HCO hematopoietic cells as well as hPSC mono/macro.

(H and I) Deduced relationship among RNA expression of day 22, day 28, and day 37 HCO hematopoietic cells; hPSC mono/macro; and a publish human fetal endodermal organ mono/macro reference dataset. Similarity score based on annotated (H) organ or (I) tissue as reference training dataset.[57] Ensemble similarity scoring based on both random forest and SVM predictions.

(J and K) UMAP clustering of macro/mono cells integrated from the day 37 HCO and the human fetal endodermal organs scRNA-seq datasets. The human fetal endodermal organ datasets were used as a reference. UMAP clustering colored by (J) organ or (K) Seurat cluster with select differential expressed markers for each cluster.

(L) Relative proportions of cells in each Seurat cluster for day 37 HCO and each fetal endodermal organ.

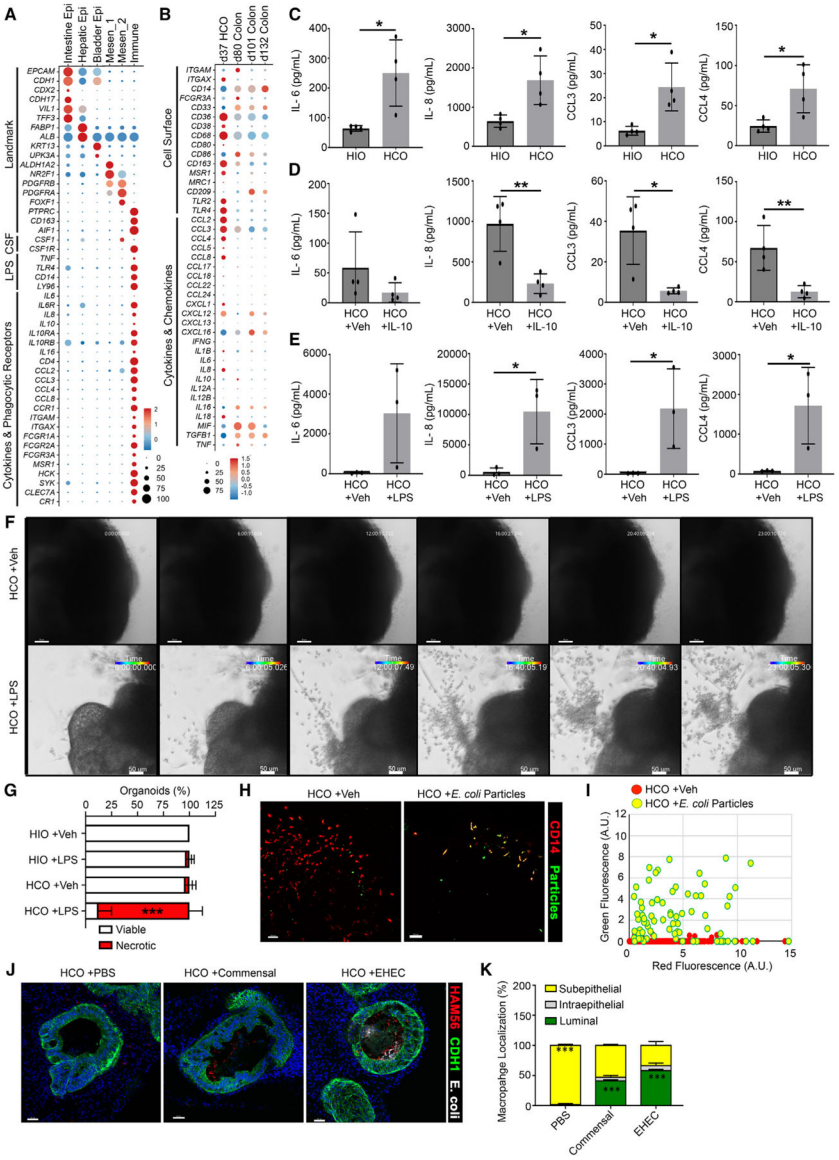


**Figure 6. HCO macrophages responded to pro- and anti-inflammatory stimuli**

(A) Relative expression of cell-type markers, as well as cytokine and phagocytic receptors in day 37 HCOs.

(B) Relative expression of cell surface markers, cytokines, and chemokines in day 37 HCO and human fetal colon macrophages.

(C–E) Luminex array data for IL-6, IL-8, CCL3, and CCL4 from paired day 35 HIO and HCO samples (from same differentiation). HCOs were (C) untreated or treated with either (D) H20 vehicle (Veh) or IL-10 for 7 days or (E) Veh or LPS for 24 h. Each point represents Luminex values from an individual differentiation (n = 3–4).

(F) Micrographs of a live imaging time course of HCOs treated with Veh/H20 or LPS of 24 h time course (see Videos S2 and S3).

(G) Quantification of HIO and HCO viability following 24 h of Veh or LPS treatment.

(H) Immunofluorescent staining of day 35 HCO with and without pHRODO *E. coli* particles (green) and CD14 macrophages (red) (see Video S4).
(I) Quantitation of phagocytosed particles into CD14+ cells in cultures treated (yellow) with *E. coli* particles or vehicle treated (red) (n = 3 wells of organoids per group).
(J) Immunofluorescent images of day 35 HCOs 24 h after the injection of PBS, commensal *E. coli*, or pathogenic EHEC stained for CDH1 (green), HAM56/MIF macrophages (red), and *E. coli* (white) counterstained with DAPI.
(K) Spatial quantitation of HAM56 macrophage distribution within the HCOs cultures (n = 3 organoids per group). Significance *p < 0.05, **p < 0.01, ***p < 0.001 determined by t tests. Scale bars: 50 μm (F, H, and J).

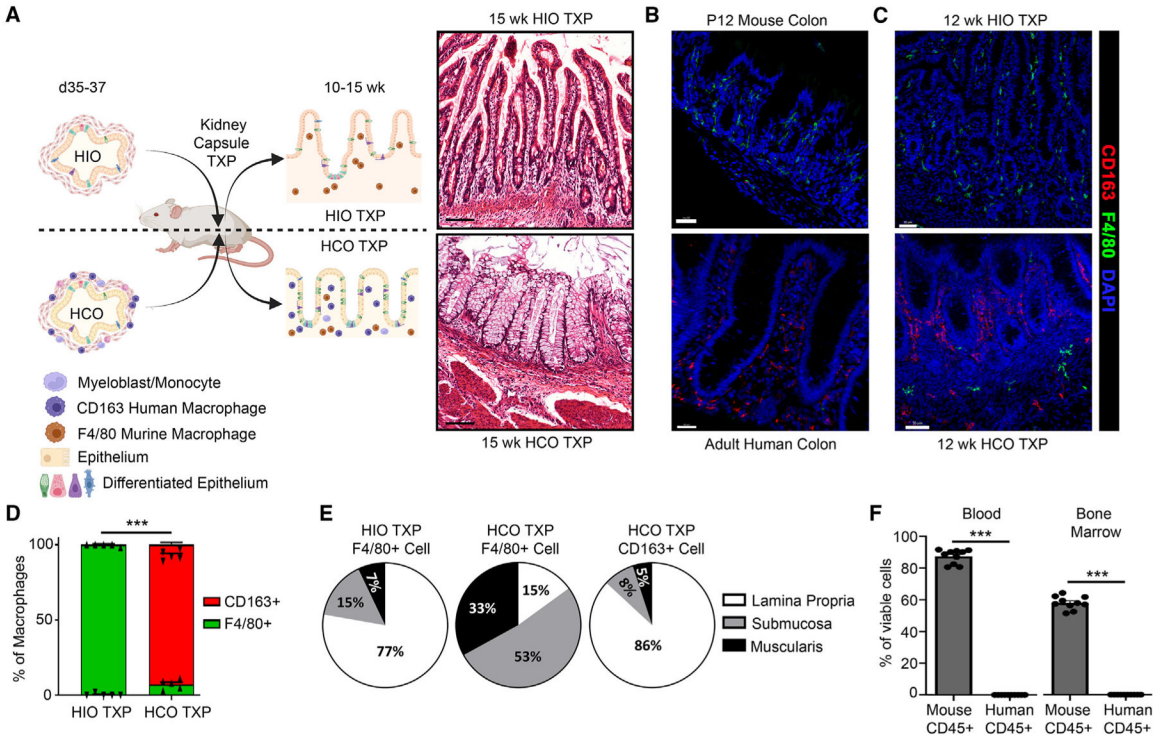


**Figure 7. HCO macrophages persisted long-term within in vivo grafts and were not displaced by bone-marrow-derived murine macrophages**

(A) Schematic of transplantation (TXP) of organoids into mouse kidney capsule and H&E images of HIO and HCO grafts following 15 weeks *in vivo*.

(B and C) Immunofluorescence of (B) mouse and human colon biopsy, and (C) 12 week HIO TXP and HCO TXP stained for human CD163 (red) and mouse-specific macrophage marker F4/80 (green) counterstained with DAPI (n = 5 transplanted organoids per condition).

(D and E) Quantification of (D) proportions of F4/80+ versus CD163+ macrophages and (E) localization of these macrophages in 12 week HIO TXP and HCO TXPs.

(F) Quantification of mouse and human CD45+ cells as a percentage of viable cells in the circulating blood and bone marrow of mice containing HCO TXP for 10–12 weeks. Graph represents mean ± SD. Significance ***$p < 0.001$ determined by unpaired t test. Scale bars: (A) 100 μm and (B and C) 50 μm.

## KEY RESOURCES TABLE

| REAGENT or RESOURCE | SOURCE | IDENTIFIER |
|---|---|---|
| Antibodies | | |
| Brilliant Violet 421 anti-human CD192 (CCR2) | BioLegend | 357209, RRID:AB_2562293 |
| APC/Fire 750 anti-human CD64 | BioLegend | 367111, RRID:AB_2566714 |
| CD14 (TuK4) FITC | Thermo Fisher Scientific | MHCD1401, RRID:AB_10373108 |
| PE/Cyanine7 anti-human CD14 | BioLegend | 367111, RRID:AB_2566713 |
| Rabbit anti-CD31 | Sigma-Aldrich | EP78, RRID:AB_2893013 |
| Rat anti-CD31 | BD Biosciences | 550274, RRID:AB_393571 |
| Mouse anti-CD34 (QBEnd/10) | Sigma-Aldrich | 134M-14, RRID:AB_1159220 |
| CD34 PE-CY7 | BD Biosciences | 560710, RRID:AB_1727470 |
| CD45 APC-CY7 | BD Biosciences | 557833, RRID:AB_396891 |
| FITC anti-human CD45 antibody | BioLegend | 368507, RRID:AB_2566367 |
| Anti-mouse CD45 Antibody PE-Cyanine5 | eBioscience | 15-0451-81, RRID:AB_468751 |
| PE anti-human TIMD4 | BioLegend | 354003, RRID:AB_11124345 |
| Rabbit anti-CD163 | Sigma-Aldrich | HPA046404, RRID:AB_2679655 |
| Goat anti-E-Cadherin (CDH1) | R&D Systems | AF648, RRID:AB_355504 |
| Mouse anti-E-Cadherin (CDH1) | BD Transduction Lab | 610182, RRID:AB_397581 |
| Rabbit anti-CDX2 (EPR2764Y) | Sigma-Aldrich | 235R-15, RRID:AB_1516799 |
| Mouse anti-CDX2 (cdx-88) | BioGenex | MU392A-UC, RRID:AB_2650531 |
| Mouse anti-human Cadherin17 | R&D Systems | MAB1032, RRID:AB_2077388 |
| Rabbit anti-Claudin18 | Sigma-Aldrich | HPA018446, RRID:AB_2669866 |
| Goat anti-SOX2 | R&D Systems | AF2018, RRID:AB_355110 |
| Goat anti-ENDOMUCIN | R&D Systems | AF4666, RRID:AB_2100035 |
| Rat anti-F4/80 (CI:A3-1) | R&D Systems | MCA497RT, RRID:AB_1102558 |
| Goat anti-GATA2 | R&D Systems | AF2046, RRID:AB_355123 |
| Mouse anti-HAM56 | Sigma-Aldrich | 279M-14, RRID:AB_1158374 |
| Rabbit Anti-RUNX1 (EPR3099) | Abcam | ab92336, RRID:AB_2049267 |
| Rabbit anti-PU.1 (SPI1) | Sigma-Aldrich | 328R-14, RRID:AB_1516986 |
| Human M-CSF Antibody | R&D Systems | MAB216, RRID:AB_2085064 |
| Donkey anti-Goat Alexa Fluor 488 | Thermo Fisher Scientific | A11055, RRID:AB_2534102 |
| Donkey anti-Goat Alexa Fluor 568 | Thermo Fisher Scientific | A11057, RRID:AB_2534104 |
| Donkey anti-Mouse Alexa Fluor 488 | Thermo Fisher Scientific | A21202, RRID:AB_141607 |
| Donkey anti-Mouse Alexa Fluor 546 | Thermo Fisher Scientific | A10036, RRID:AB_2534012 |
| Donkey anti-Mouse Alexa Fluor 647 | Thermo Fisher Scientific | A31571, RRID:AB_162542 |
| Donkey anti-Rabbit Alexa Fluor 488 | Thermo Fisher Scientific | A21206, RRID:AB_2535792 |
| Donkey anti-Rabbit Alexa Fluor 546 | Thermo Fisher Scientific | A10040, RRID:AB_2534016 |
| Donkey anti-Rabbit Alexa Fluor 647 | Thermo Fisher Scientific | A31573, RRID:AB_2536183 |
| Donkey anti-Rat Alexa Fluor 488 | Thermo Fisher Scientific | A21208, RRID:AB_2535794 |
| Anti-Human CD45-141Pr | Fluidigm | 3141009B |
| Anti-Human CD11b/Mac-1-144Nd | Fluidigm | 3144001B, RRID: AB_2714152 |

| REAGENT or RESOURCE | SOURCE | IDENTIFIER |
|---|---|---|
| Anti-Human CD14-175Lu | Fluidigm | 3175015B, RRID:AB_2811083 |
| Anti-Human CD16-165Ho | Fluidigm | 3165001B, RRID: AB_2802109 |
| Bacterial and virus strains | | |
| *E. coli* Commensal | Weiss Lab University of Cincinnati | SGUC183 |
| *E. coli* Enterohemorrhagic | Weiss Lab University of Cincinnati | O157:H7, PT29S |
| Biological samples | | |
| Human Colon Biopsies | Yacyshyn Lab University of Cincinnati | M02 and M03 |
| Chemicals, peptides, and recombinant proteins | | |
| Activin A | Cell Guidance Systems | GFH6 |
| Accutase | Thermo Fisher Scientific | A11105-01 |
| Advanced DMEM:F12 | Thermo Fisher Scientfic | 12634-010 |
| B27 supplement w/o Vitamin A (50x) [1x] | Thermo Fisher Scientific | 12587-010 |
| Bovine serum albumin (BSA) [1%] | VWR | 10842-772 |
| Cell Recovery Solution | Corning | 354253 |
| FITC-Dextran | Sigma-Aldrich | FD4 |
| pHrodo Green *E. coli* BioParticles | Life Technologies | P35366 |
| 7-Aminoactinomycin D (7-AAD) | Invitrogen | A1310 |
| SYTOX Blue | Thermo Fisher Scientific | S34857 |
| DAPI | Sigma-Aldrich | D9542 |
| CHIR99021 [3 μM] | ReproCell | 04-0004-10 |
| Defined fetal bovine serum (dFBS) | Hyclone | SH30070.02 |
| Dispase | Thermo Fisher Scientific | 17105-041 |
| DMEM:F12 | Thermo Fisher Scientific | 11320033 |
| Fetal bovine serum | Sigma Aldrich | 12306C |
| Gelatin [0.1%] | Stem Cell Technologies | 7903 |
| HEPES Buffer | Thermo Fisher Scientific | 15630080 |
| hESC-qualified Matrigel | BD Biosciences | 354277 |
| L-glutamine (100x) [1x] | Thermo Fisher Scientific | 25030-081 |
| Lipopolysaccharide (LPS) from *E. coli* K12 Ultrapure | Invitrogen | tlrl-peklps |
| Matrigel Matrix Basement Membrane | BD Biosciences | 354234 |
| mTeSR1 media | Stem Cell Technologies | 5850 |
| N2 Supplement (100x) [1x] | Thermo Fisher Scientific | 17502-048 |
| Non-essential Amino Acids (100x) [1x] | Thermo Fisher Scientific | 11140050 |
| Normal donkey serum | Jackson ImmunoResearch Laboratories | 017-000-121 |
| Pen/Strep (100x) | Thermo Fisher Scientific | 15140-122 |
| recombinant human bFGF2 | R&D Systems | 233-FB-500 |
| recombinant human BMP2 | R&D Systems | 355-BM-050 |
| recombinant human BMP4 | R&D Systems | 314-BP-050 |
| recombinant human GM-CSF | R&D Systems | 215-GM-050 |

| REAGENT or RESOURCE | SOURCE | IDENTIFIER |
|---|---|---|
| recombinant human M-CSF | R&D Systems | 216-MC-025 |
| recombinant human EGF | R&D Systems | 236-EGF-01M |
| recombinant human FGF4 | R&D Systems | 235-F4 |
| recombinant human IL-10 | R&D Systems | 217-IL-005 |
| recombinant human NOGGIN | R&D Systems | 6057-NG |
| TransIT-LT1 Transfection Reagent | Mirus Bio | MIR2300 |
| TrypLE Select Enzyme | Thermo Fisher Scientific | 12563029 |
| Trypsin-EDTA (0.25%) | Thermo Fisher Scientific | 25200056 |
| Y-27632 dihydrochloride | Tocris | 1254 |
| Critical commercial assays | | |
| Quantitect SYBR Green | Qiagen | 204145 |
| NucleoSpin RNA | Macherey-Nagel | 740955 |
| SuperScript VILO cDNA Synthesis Kit | Thermo Fisher Scientific | 11754250 |
| Methocult H4434 Classic Methylcellulose Medium Human | StemCell Technologies | 04444 |
| Luminex Array ELISA IL-6, IL-8, CCL3, CCL4, TNFa | R&D Systems | FCSTM18 |
| Differential Quik modified Giemsa | Electron Microscopy Sciences | 26096 |
| Neural Tissue Dissociation Kit | Miltenyi Biotec | 130-092-628 |
| STEMdiff Hematopoietic Kit | StemCell Technologies | 05310 |
| Deposited data | | |
| Raw and analyzed bulk RNA-seq data - *in vitro* HIOs and HCOs d10. | Múnera et al.[36] | ArrayExpress: E-MTAB-5658 |
| Raw and analyzed bulk RNA-seq data - *in vitro* HIOs and HCOs d21 and d35. | This Paper | GEO: GSE240363 |
| Raw and analyzed bulk RNA-seq data - *in vitro* HIO (mod), HCO (mod) and HCOs d35. | This Paper | GEO: GSE240363 |
| Raw and analyzed scRNA-seq data - *in vitro* HCO d22 and d37 | This Paper | GEO: GSE240363 |
| Raw and analyzed scRNA-seq data - *in vitro* HCO hematopoietic suspended cells only d28 | This Paper | GEO: GSE240363 |
| Raw and analyzed scRNA-seq data - *in vivo* HCO transplant 15 wks post-transplant | This Paper | GEO: GSE240363 |
| Raw and analyzed scRNA-seq data - *in vitro* iPSC-derived Monocyte/Macrophages d14 | This Paper | GEO: GSE240363 |
| Reference scRNA-seq data - human fetal hemogenic and hematopoietic atlas | Calvanese et al.[16] | GEO: GSE162950 |
| Reference scRNA-seq data - human fetal hematopoietic atlas | Popescu et al.[51] | ArrayExpress: E-MTAB-7407 |
| Reference scRNA-seq data - human fetal hematopoietic and macrophage atlas | Bian et al.[15] | GEO: GSE133345 |
| Reference scRNA-seq data - human fetal endodermal organ atlas | Yu et al.[57] | ArrayExpress: E-MTAB-10187, E-MTAB-10268, E-MTAB-8221, E-MTAB-9228, E-MTAB-9489 |
| Experimental models: Cell lines | | |

| REAGENT or RESOURCE | SOURCE | IDENTIFIER |
|---|---|---|
| Human: H1 ES cells | CCHMC Pluripotent Stem cell core / WiCell Research Institute | NIH hESC-10-0043 |
| Human: iPSC72.3 iPS cells | CCHMC Pluripotent Stem cell core/ McCracken et al.[35] | N/A |
| Human: iPSC115.3 iPS cells | CCHMC Pluripotent Stem cell core / This Paper | N/A |
| Human: iPSC209.2 iPS cells | CCHMC Pluripotent Stem cell core / This Paper | N/A |
| Human: iPSC263.10 iPS cells | CCHMC Pluripotent Stem cell core / Holokai et al.[90] | N/A |
| Human: HEK-293T | CCHMC Pluripotent Stem cell core / ATCC | CRL-3216 |
| Mouse: Irradiated CF1-MEF Feeders | CCHMC Pluripotent Stem cell core | N/A |
| Experimental models: Organisms/strains | | |
| Mouse: NSG (NOD.Cg-PrkdcscidIl2rgtm1Wjl/SzJ) | CCHMC Comprehensive Mouse and Cancer Core Facility | N/A |
| Mouse: Wildtype CD1 Mice | Charles River | 022 |
| Oligonucleotides | | |
| CDX2 gRNA Target Sequence: GTCGCTACATCACCATCCGG | http://CRISPOR.org/ Integrated DNA Technologies (IDT) / This Paper | N/A |
| RT-PCR Primer Sequences | See Table S2 | N/A |
| Recombinant DNA | | |
| Plasmid: High Fidelity modified pX458-eSPCas9(1.1)-2A-GFP | CCHMC Genome Editing Core | Addgene Plasmid #48138 |
| Software and algorithms | | |
| Bowtie | Langmead et al.[91] | v2.2.5 |
| Cufflinks | Trapnell et al.[92] | v2.2.1 |
| Debian Linux 64-bit “Wheezy” | N/A | v7.10 |
| FastQC | N/A | v0.10.1 |
| Partek® Flow® | N/A | N/A |
| IMARIS | Bitplane | N/A |
| NIS Elements | Nikon | N/A |
| R | N/A | v3.6.3, v4.1.1, and v4.2.1 |
| R Studio | N/A | v1.2.5033 and v1.4.1717 |
| Seurat | Butler et al.[93] | v3.2.1 |
| TopHat | N/A | v2.0.13 |
| CellRanger | 10x Genomics | v3.0.2 |
| FACSDiva | BD Biosciences | N/A |
| Monocle 3 | Cao et al.[94] | v1.2.7 |
| CellChat | Jin et al.[95] | v1.1.3 |
| ELeFHAnt | Thorner et al.[96] | v1.1.4 |

| REAGENT or RESOURCE | SOURCE | IDENTIFIER |
|---|---|---|
| Prism 9 | Graphpad | v9.5.1 |
| Other | | |
| Ultra-Low Attachment Plates | Corning | 3471 |
| AggreWell 400 24 well Plates | StemCell Technologies | 34415 |
| Ibidi 2 well chambers | Ibidi | 80286 |